

Quantitative comparison of electron temperature fluctuations to nonlinear gyrokinetic simulations in C-Mod Ohmic L-mode discharges

C. Sung^{*}, A. E. White, D. R. Mikkelsen, M. Greenwald, C. Holland, N. T. Howard, R. Churchill, C. Theiler, and Alcator C-Mod Team

Citation: *Physics of Plasmas* **23**, 042303 (2016); doi: 10.1063/1.4945620

View online: <http://dx.doi.org/10.1063/1.4945620>

View Table of Contents: <http://aip.scitation.org/toc/php/23/4>

Published by the *American Institute of Physics*

Articles you may be interested in

[Synergistic cross-scale coupling of turbulence in a tokamak plasma](#)

Physics of Plasmas **21**, 112510 (2014); 10.1063/1.4902366

[Multi-scale gyrokinetic simulations: Comparison with experiment and implications for predicting turbulence and transport](#)


Physics of Plasmas **23**, 056109 (2016); 10.1063/1.4946028

[Multi-channel transport experiments at Alcator C-Mod and comparison with gyrokinetic simulations](#)

Physics of Plasmas **20**, 056106 (2013); 10.1063/1.4803089

[Measurements of the cross-phase angle between density and electron temperature fluctuations and comparison with gyrokinetic simulations](#)

Physics of Plasmas **17**, 056103 (2010); 10.1063/1.3323084



Small Conferences. BIG Ideas.

Applied Physics Reviews

SAVE THE DATE!

3D Bioprinting: Physical and Chemical Processes

May 2–3, 2017 • Winston Salem, NC, USA

Quantitative comparison of electron temperature fluctuations to nonlinear gyrokinetic simulations in C-Mod Ohmic L-mode discharges

C. Sung,^{1,a)} A. E. White,² D. R. Mikkelsen,³ M. Greenwald,² C. Holland,⁴ N. T. Howard,² R. Churchill,³ C. Theiler,⁵ and Alcator C-Mod Team²

¹University of California, Los Angeles, Los Angeles, California 90095, USA

²Plasma Science and Fusion Center, Massachusetts Institute of Technology, Cambridge, Massachusetts 02139, USA

³Princeton Plasma Physics Laboratory, Princeton, New Jersey 08543, USA

⁴University of California, San Diego, La Jolla, California 92093, USA

⁵Ecole Polytechnique Fédérale de Lausanne, SPC, Lausanne 1015, Switzerland

(Received 25 January 2016; accepted 18 March 2016; published online 8 April 2016)

Long wavelength turbulent electron temperature fluctuations ($k_y \rho_s < 0.3$) are measured in the outer core region ($r/a > 0.8$) of Ohmic L-mode plasmas at Alcator C-Mod [E. S. Marmor *et al.*, Nucl. Fusion **49**, 104014 (2009)] with a correlation electron cyclotron emission diagnostic. The relative amplitude and frequency spectrum of the fluctuations are compared quantitatively with nonlinear gyrokinetic simulations using the GYRO code [J. Candy and R. E. Waltz, J. Comput. Phys. **186**, 545 (2003)] in two different confinement regimes: linear Ohmic confinement (LOC) regime and saturated Ohmic confinement (SOC) regime. When comparing experiment with nonlinear simulations, it is found that local, electrostatic ion-scale simulations ($k_y \rho_s \lesssim 1.7$) performed at $r/a \sim 0.85$ reproduce the experimental ion heat flux levels, electron temperature fluctuation levels, and frequency spectra within experimental error bars. In contrast, the electron heat flux is robustly under-predicted and cannot be recovered by using scans of the simulation inputs within error bars or by using global simulations. If both the ion heat flux and the measured temperature fluctuations are attributed predominantly to long-wavelength turbulence, then under-prediction of electron heat flux strongly suggests that electron scale turbulence is important for transport in C-Mod Ohmic L-mode discharges. In addition, no evidence is found from linear or nonlinear simulations for a clear transition from trapped electron mode to ion temperature gradient turbulence across the LOC/SOC transition, and also there is no evidence in these Ohmic L-mode plasmas of the “Transport Shortfall” [C. Holland *et al.*, Phys. Plasmas **16**, 052301 (2009)]. © 2016 AIP Publishing LLC. [<http://dx.doi.org/10.1063/1.4945620>]

I. INTRODUCTION

Anomalous electron heat transport levels, higher than neoclassical transport levels, in tokamak experiments are one of the main barriers toward fusion energy production. There is a great deal of evidence both experimentally and theoretically that drift-wave turbulence at the ion and electron scales is responsible for this anomalous transport.¹ The nonlinear gyrokinetic model has been used extensively to study the turbulent transport in tokamak plasmas, with recent papers focusing on validation efforts that involve direct comparisons with measured turbulence.^{2–8} Validation of the gyrokinetic model is an important step towards using this model for assessing the performance of fusion plasmas in the future.

In general, at Alcator C-Mod,⁶² the heat transport in Ohmic L-mode discharges has proven to be very challenging to model with nonlinear gyrokinetic simulations.^{9,10} In addition, there are several interesting transport observations in Alcator C-Mod Ohmic discharges that appear to occur together, highlighting the complex nature of coupled transport channels. At C-Mod, it is found that the intrinsic rotation reversal, changes in poloidal asymmetry of impurity

density, and the occurrence of non-local heat transport, along with a strong reduction of measured long wavelength electron temperature fluctuations, occur concomitantly across the Ohmic confinement transition (LOC/SOC transition).^{11,12} It has been suggested that a unifying hypothesis for these changes is a change in the underlying turbulence from dominant trapped electron mode (TEM) to ion temperature gradient (ITG) across the LOC/SOC transition,^{11,12} which will be a continuous transition in terms of their relative amplitudes, not discrete, in reality. There is counter evidence from C-Mod¹³ and from ASDEX Upgrade,¹⁴ suggesting that the LOC/SOC transition occurs without a change in turbulence from TEM to ITG. It is also noteworthy that we do not understand clearly all these changes are coupled together. The changes in impurity density can be correlated with the intrinsic core rotation reversal since the centrifugal force will change with the core rotation changes. Although rotation reversal occurs robustly with the LOC/SOC transition in C-Mod,¹⁵ it has been also observed that these two phenomena are not correlated in Tore-Supra¹⁶ and ASDEX-Upgrade.^{14,17} These conflicting observations motivated the current work.

In addition to studying the physics of the LOC/SOC transition, validation of gyrokinetic codes in a variety of plasmas is of interest. Ohmic L-mode plasmas may require less

^{a)}csung@physics.ucla.edu

modeling effort compared to externally heated L- and H-mode plasmas since we do not consider external heating profile from RF heating or neutral beam injection (NBI) and fast ion density profile due to external heating. On the other hand, the normalized heat flux by a gyroBohm value will be higher in Ohmic L-mode discharges, which makes harder in the comparison of the gyrokinetic simulation results with the experiments due to the higher dependence on the stiffness level. Thus, these Ohmic L-mode plasmas are good targets for validation study. Past work with GYRO¹⁸ local nonlinear simulations of LOC/SOC plasmas at C-Mod was performed only inside the $r/a < 0.8$ region.⁹ Over the core region, $r/a = [0.4, 0.8]$, the past work found that the ion heat diffusivity was under-predicted and electron heat diffusivity was over-predicted compared to the experimental values (estimated from power balance analysis using a time dependent transport analysis code (TRANSP)¹⁹). In contrast, the line-integrated electron density fluctuations measured by phase contrast imaging (PCI) agreed with the simulations. The discrepancy in core heat transport is still being investigated at C-Mod, and a recent paper has found that the discrepancies remain even when using global simulations.¹⁰

To the past work at C-Mod, we add newly available measurements of long wavelength electron temperature fluctuations from a correlation electron cyclotron emission (CECE) diagnostic.^{13,20,21} These new data provide an additional constraint on the simulations. The outer core region, $r/a > 0.8$, has not been investigated in the past using gyrokinetic simulations in Ohmic L-mode plasmas at C-Mod, so we focus on this region. We use nonlinear GYRO simulations constrained by CECE measurements to explore the hypothesis that the LOC/SOC transition is related to changes in the underlying turbulence, specifically, a change from TEM to ITG turbulence. And in addition, our results also address the so-called ‘‘Transport Shortfall’’³ in this region. We note that the ‘‘Shortfall’’ is seen in DIII-D NBI L-mode plasmas with the GYRO³ and GEM⁶ codes but is not seen in C-Mod RF L-mode plasmas with the GYRO code²² or in ASDEX Upgrade NBI L-mode plasmas with the GENE code.²³ It is also noteworthy that ‘‘Shortfall’’ is seen in even DIII-D NBI L-mode discharge with the GENE.⁷ The validation study presented here for the outer core region ($r/a > 0.8$) of C-Mod Ohmic L-mode plasmas may help identify differences seen across machines and codes.

In Section II, we summarize the experimental results, the preparation of experimental data for input to the gyrokinetic code, and linear stability analysis results using experimental profiles as input. In Section III, we describe the set-up for nonlinear gyrokinetic simulations and the synthetic CECE diagnostic. In Section IV, results from the nonlinear simulations are compared with experiment and the hypothesis of changes in turbulence from TEM to ITG across the LOC/SOC transition is explored. Section V presents a discussion and summary.

II. EXPERIMENTAL RESULTS

A. Changes in turbulence and transport across the LOC/SOC transition

The two C-Mod Ohmic discharges that we use for the validation study have been reported on previously, and

extensive measurements of the electron temperature fluctuations in general in Ohmic L-mode plasmas at C-Mod have been described in detail elsewhere.¹³ In this paper, two plasmas are modeled with gyrokinetic simulations. One discharge is in the linear ohmic confinement (LOC) regime and the other is in the saturated ohmic confinement (SOC) regime, with line-integrated density, $\bar{n}_e = 0.5 \times 10^{20} \text{ m}^{-2}$ for LOC and $\bar{n}_e = 0.8 \times 10^{20} \text{ m}^{-2}$ for SOC. The discharges had the same toroidal magnetic field, $B_t = 5.4 \text{ T}$ in co-current direction, plasma current, $I_p \sim 0.9 \text{ MA}$, and Ohmic power, $P_{oh} \sim 1 \text{ MW}$, in lower single null (LSN) configuration with the same geometry, $R = 0.67 \text{ m}$, $a = 0.22 \text{ m}$, $\kappa = 1.6$, $\delta_l = 0.54$, $\delta_u = 0.26$. The estimated main ion fraction (n_D/n_e) is $0.82(\pm 0.09)$ for the LOC and $0.95(\pm 0.03)$ for the SOC discharges. The confinement regime of each discharge was determined by the direction of toroidal rotation.¹⁵ The discharges are selected for comparison with gyrokinetic simulations because the plasma parameters are very stationary for long time periods, between $t = 0.9$ and $t = 1.4 \text{ s}$.

In the LOC/SOC Ohmic discharges, time-averaged ($t = 0.9\text{--}1.4 \text{ s}$) long wavelength electron temperature fluctuations were measured at $r/a \sim 0.85$. These measurements are made with a multi-channel correlation electron cyclotron emission (CECE) diagnostic, which is sensitive to turbulence with normalized wavenumbers, $k_y \rho_s < 0.3$, where k_y is the poloidal wave number and ρ_s is the sound gyroradius of main ion, defined as $\rho_s = c_s/\Omega_{ci}$ with $c_s = \sqrt{T_e/m_i}$ and $\Omega_{ci} = eB/m_i c$. CECE is a standard technique used to measure electron temperature fluctuations in tokamaks, having been deployed previously at several different devices^{2,24,25} and compared with nonlinear gyrokinetic simulations in a number of studies.^{3,6,7} Details of the CECE diagnostic as implemented at C-Mod are found in Refs. 13 and 20. The CECE measurements provide the relative fluctuation level and the frequency spectrum of the long wavelength temperature fluctuations in the two plasmas. These two measured quantities can be compared directly using a synthetic CECE diagnostic applied to outputs from the GYRO code.³ Details of the synthetic diagnostic used in this work can be found in Ref. 26, but it is noteworthy that full T_e fluctuations were used in this study rather than the perpendicular T_e fluctuations as used in Ref. 7. CECE measurements have been made in many Ohmic L-mode plasmas, and in general, across LOC/SOC transition at C-Mod we have observed that the electron temperature fluctuation level at $r/a \sim 0.85$ decreases. In Figure 1, the measured electron temperature fluctuation level decreases 30% from 1.0% to 0.7%.¹³ In contrast, line integrated density fluctuations measured with the PCI diagnostic (not shown here) in the same experiments did not show a decrease in fluctuation level.¹³

The turbulence relevant profiles for the LOC and SOC discharges averaged over $t = 0.9\text{--}1.4 \text{ s}$ are shown in Fig. 2. The solid line in this figure shows the experimental value and the dotted line represents the uncertainty in the measured profiles. The green vertical line indicates the CECE measurement position (cold resonance position of the measured electron cyclotron (EC) radiation). Electron collisionality, ν_e^* , shown in Fig. 2(i), is defined as $\nu_e^* = \frac{\nu_e}{\omega_{be}}$, where ν_e is the electron ion collision frequency, defined as

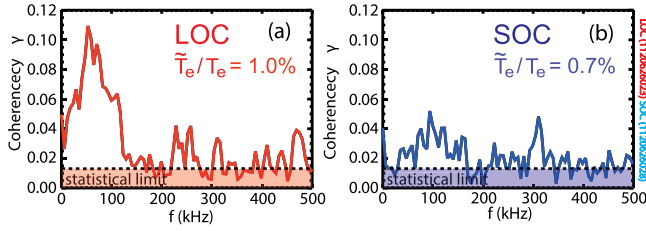


FIG. 1. Time averaged ($t=0.9\text{--}1.4\text{ s}$) \tilde{T}_e/T_e fluctuations measured with CECE in an LOC (red) and an SOC (blue) discharge at $r/a \approx 0.85$. The fluctuation level is found from integrating the spectrum between $f=0\text{--}170\text{ kHz}$. In LOC, the relative fluctuation level is higher, $\tilde{T}_e/T_e \approx 1.0\%$, than in SOC $\tilde{T}_e/T_e \approx 0.7\%$.

$\nu_e = 2.91 \times 10^{-6} n_e [\text{cm}^{-3}] \ln \Lambda T_e [\text{eV}]^{-3/2} [\text{Hz}]$ with the Coulomb logarithm, $\ln \Lambda$, and $\omega_{b,e}$ is the electron bounce frequency, defined as $\omega_{b,e} = \epsilon^{1/2} \frac{v_e}{qR}$ with the inverse aspect ratio, ϵ , the velocity of electron, v_e , and the safety factor, q .²⁷ The collisionality was calculated from TRANSP¹⁹ and

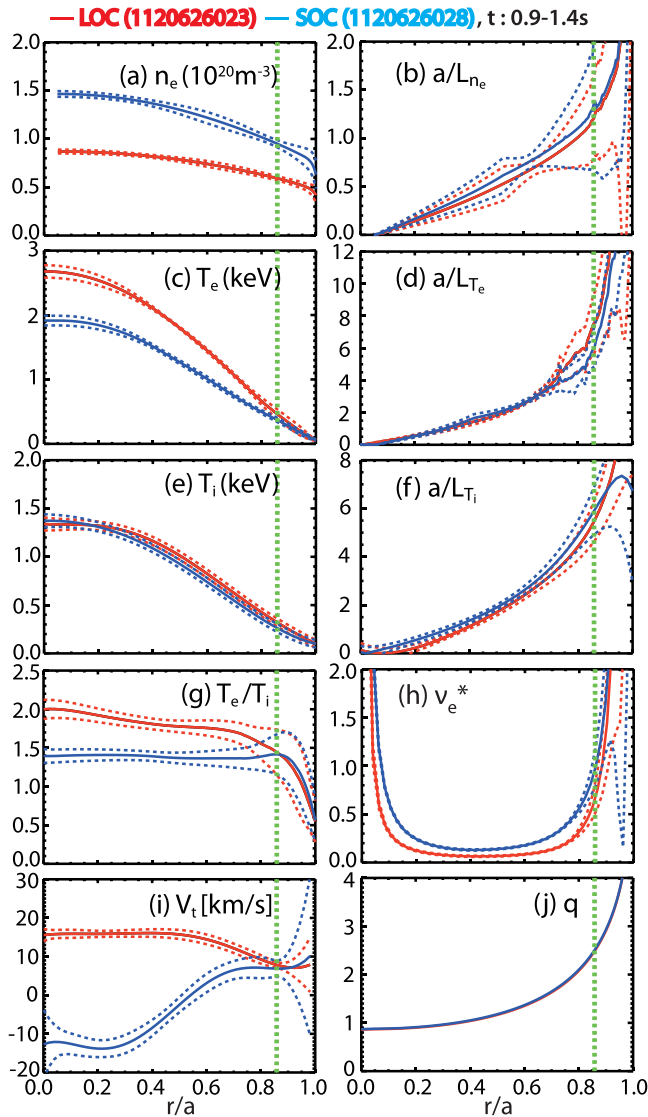


FIG. 2. Profiles relevant to turbulence and CECE measurements in the LOC/SOC discharges (1120626023 LOC red and 1120626028 SOC blue). The solid line shows the experimental value and the dotted line indicates the uncertainty. The vertical green line shows the CECE measurement position in these plasmas.

its uncertainty was obtained from the standard deviation of time-averaged profiles. The safety factor, q , profile (Fig. 2(j)) was obtained from the equilibrium reconstruction constrained by magnetic diagnostics via the equilibrium code (EFIT).²⁸ The estimated uncertainty of the safety factor, q , profile from time averaging was less than 5% in these sawtooth discharges and is not shown on the plot of the q profile in Fig. 2.

As shown in Fig. 2, the SOC discharge has higher electron density and lower electron temperature in the whole radial region except for the edge region ($r/a > 0.9$) where the T_e values in the SOC plasma are similar to the values in the LOC within the uncertainty. The higher n_e and lower T_e make the SOC discharge more collisional than the LOC discharge in the core region as shown in Fig. 2(h). Ion temperature is similar between LOC/SOC plasmas in the whole radial region. Consequently, the ratio T_e/T_i is lower in the SOC discharge compared to the LOC discharge. There was no significant difference (i.e., outside of uncertainties), between the LOC/SOC discharges in gradient scale lengths and safety factor, q .

Because the reversal of the intrinsic rotation, core toroidal rotation is in opposite directions (co-current in LOC and counter-current in SOC). Estimating the correct rotation frequency, ω_o , and $E \times B$ shearing rate, $\gamma_{E \times B}$, can be crucial to the validation study of gyrokinetic simulation. This is because the measured lab-frame frequency spectrum of the fluctuations will be spread in frequency and shifted to higher frequency due to the Doppler effect. The radial gradient of the toroidal velocity will affect the $E \times B$ shearing rate and thus can play a role in turbulence suppression. The rotation profiles shown in Fig. 2 are used to estimate ω_o and $\gamma_{E \times B}$.

It is noteworthy that all parameters shown in Fig. 2 except for collisionality are similar within the uncertainty at the CECE measurement position, $r/a \approx 0.85$. Higher collisionality in the SOC regime will reduce the response of non-adiabatic electrons, which are mostly trapped electrons. Since temperature fluctuations arise from the non-adiabatic electrons' response, it is tempting to link the reduced fluctuation levels with a reduction of TEM turbulence in the SOC plasma. However, the change in CECE measured temperature fluctuations does not necessarily imply a change of dominant turbulent mode from TEM to ITG across the LOC/SOC transition, as suggested by past authors.^{29–31} This is because non-adiabatic electrons can destabilize the ITG mode as well,^{32,33} and hence, temperature fluctuations at long wavelength could change as the ITG turbulence evolves (while remaining “ITG-type”). We also note that the LOC plasma is more diluted by impurities than the SOC plasma as mentioned above ($n_D/n_e = 0.82(\pm 0.09)$ for the LOC and $0.95(\pm 0.03)$ for the SOC). Having more impurities (a lower main ion fraction, n_D/n_e) in the LOC discharge will help stabilize ITG turbulence.^{10,34,35} It might be expected then that the ITG mode will be less stable in the SOC discharge, which would be consistent with reduced turbulence and transport. However, while temperature fluctuations are reduced across the LOC/SOC transition, the density fluctuations measured with PCI do not change.¹³ The effect of both

collisionality and dilution in these plasmas will be probed using the gyrokinetic simulations.

As a first step at characterizing the expected turbulence in these plasmas, linear stability analysis is carried out with GYRO using the experimental profile values as input. Figure 3 shows the eigenvalue linear stability analysis results, which are used to track not only the fastest growing mode but also changes in subdominant modes. Figure 3 shows the most unstable electron mode (dotted line) and the most unstable ion mode (dashed line). Additional unstable ion and electron roots were also found in this analysis (not shown in Fig. 3). For the LOC plasma at ($r/a \sim 0.85$), Fig. 3(a) shows that both an electron mode and an ion mode are unstable over the range $k_y \rho_s < 1.0$, with an electron mode most dominant in the range $k_y \rho_s < 0.3$, where CECE is most sensitive to temperature fluctuations. For the SOC plasma at ($r/a \sim 0.85$), Fig. 3(b) shows again that both electron and ion modes are unstable over the range $k_y \rho_s < 1.0$, and in the

range $k_y \rho_s < 0.3$, where CECE is most sensitive to temperature fluctuations, the fastest growing mode has a real frequency very close to zero. The linear stability analysis shows that the plasmas are fairly described as “mixed mode,” with both TEM and ITG modes strongly unstable at long wavelength. From this analysis, there is no clear evidence that the LOC plasma is strongly TEM dominant and the SOC plasma is strongly ITG dominant at $r/a = 0.85$. We note that this is in agreement with past linear stability analysis at the same radius,^{11–13} and that deeper in the core, $r/a = 0.6$, linear stability shows that ITG is strongly dominant, with little to no subdominant TEM in both the LOC and SOC plasmas.^{9,13} However, this analysis result does not mean that there is no change in turbulence across the LOC/SOC transition. In Fig. 3, we can also see that the growth rate of the most unstable electron mode in $k_y \rho_s > 0.4$ decreases across the LOC/SOC transition. This will be discussed more later in this paper.

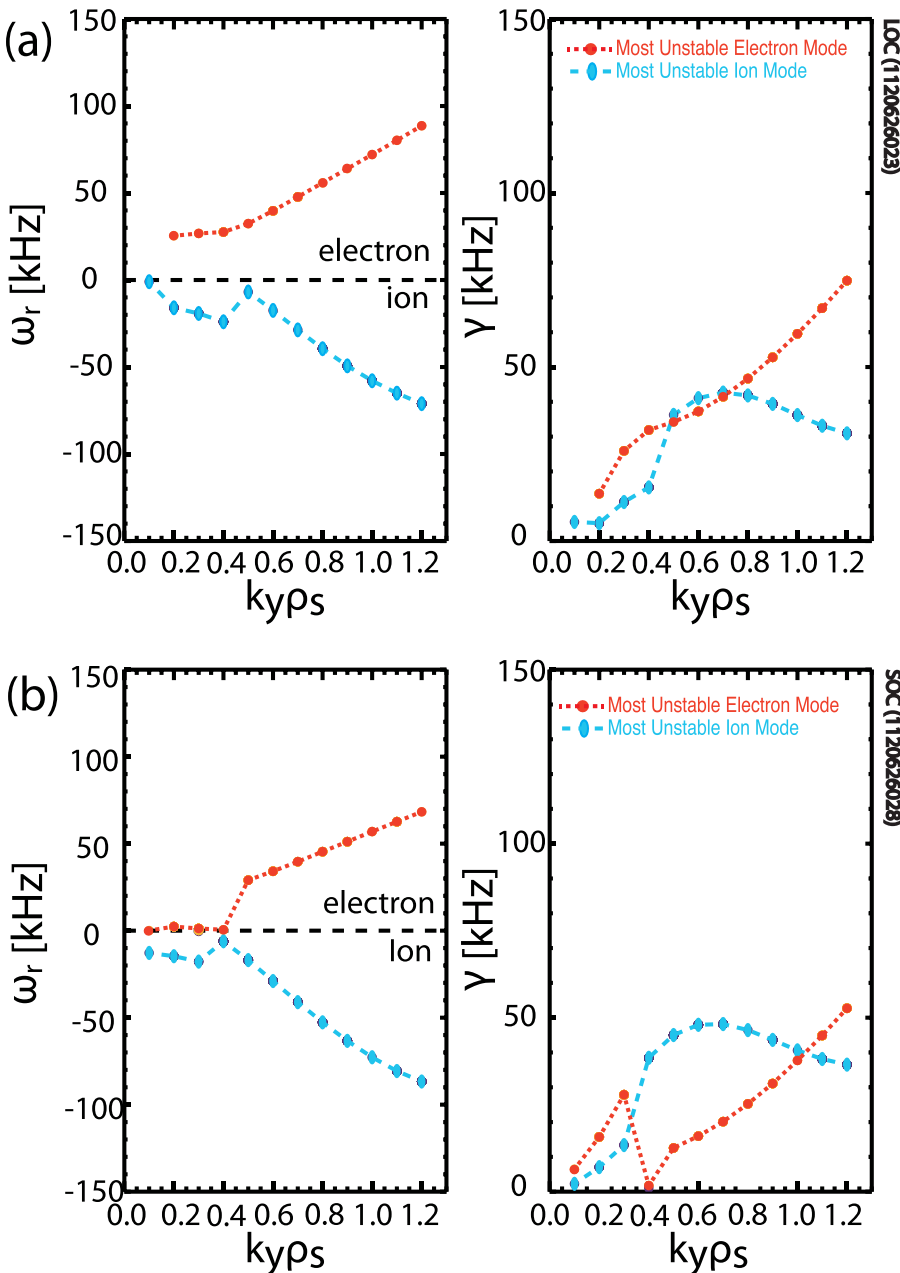


FIG. 3. Linear stability analysis using the GYRO eigenvalue solver with experimental values for (a) the LOC discharge (shot 1120626023) and (b) the SOC discharge. Color codes are used in this figure as follows. red-circles, dotted line: Most unstable electron mode, blue-ovals, dashed line: most unstable ion mode.

The experimental electron/ion heat diffusivities and fluxes for the LOC/SOC plasmas are found through power balance analysis using TRANSP.¹⁹ The resulting heat fluxes and thermal diffusivities are shown in Figure 4. These are time-averaged during the steady periods of interest ($t = 0.9\text{--}1.4$ s), and their uncertainties are estimated by considering the uncertainties of the dominant terms in the power balance analysis through error propagation.²⁶ As shown in Figure 4, the SOC plasma has lower electron thermal heat diffusivity and flux than the LOC plasma, while ion heat diffusivity and heat flux in the SOC plasma are higher in the whole radial region outside the sawtooth inversion radius (~ 0.4) although their differences are within the uncertainty except for the ion heat flux. This result is consistent with similar analysis performed in the past in FTU³⁶ and C-Mod,⁹ but inconsistent with the result in Tore Supra.³⁷

III. NONLINEAR GYROKINETIC SIMULATION SET-UP

In this study, local gyrokinetic simulations were performed for the LOC and SOC discharges at the CECE measurement position ($r/a \sim 0.85$) to compare with the experimental heat transport values and the temperature fluctuation measurements. We ran global simulations as well and found that the results agreed with the local simulations because of the small ρ^* value. The local and global simulations have been compared in detail elsewhere,²⁶ so here we describe only the local simulation results.

Table I shows the input parameters used in the local gyrokinetic simulations, performed at $r/a \sim 0.85$. The input values given here are for the GYRO “base case” runs for LOC (shot 1120626023) and SOC (shot 1120626028) at the CECE measurement position (~ 0.85). The values are time averaged over 0.5 s (0.9–1.4 s). These experimental values are taken from the profile data shown in Fig. 2 (unless noted). Here $\rho^* = \rho_s/a$ with sound gyroradius of the main ion (Deuterium) ρ_s and minor radius, a . It is noteworthy that $B_{\text{unit}} (= \frac{1}{r} \frac{d\chi_i}{dr}$ with toroidal flux, χ_i) is used to calculate ρ_s in

TABLE I. Experimental parameters and input values for the GYRO “base case” runs for LOC (shot 1120626023) and SOC (shot 1120626028) at CECE measurement position ($r/a \approx 0.85$). The values are time averaged over 500 ms from $t = 0.9\text{--}1.4$. In the “base case” columns, only input parameters that were changed from the experimental values (the $E \times B$ shear and density gradient scale length) are listed. All other inputs were taken as the experimental values.

	LOC experimental	SOC experimental	LOC base case	SOC base case
ρ^*	1.5×10^{-3}	1.4×10^{-3}
c_s/a (MHz)	0.65	0.59
n_e (10^{20}m^{-3})	$0.58 (\pm 0.022)$	$0.94 (\pm 0.036)$
a/L_{n_e}	$1.25 (\pm 0.45)$	$1.30 (\pm 0.57)$...	1.87
T_e (keV)	$0.43 (\pm 0.068)$	$0.35 (\pm 0.030)$
a/L_{T_e}	$7.48 (\pm 1.84)$	$6.28 (\pm 1.16)$
T_i (keV)	$0.31 (\pm 0.040)$	$0.25 (\pm 0.039)$
a/L_{T_i}	$5.54 (\pm 0.84)$	$5.86 (\pm 0.95)$
$T_e T_i$	$1.39 (\pm 0.28)$	$1.40 (\pm 0.25)$
Z_{eff}	$2.53 (\pm 0.47)$	$1.48 (\pm 0.25)$
n_D/n_e	$0.82 (\pm 0.09)$	$0.95 (\pm 0.03)$
n_B/n_e	$0.036 (\pm 0.018)$	$0.01 (\pm 0.006)$
ν_{ei} [c_s/a]	$0.56 (\pm 0.11)$	$1.28 (\pm 0.22)$
ω_o [c_s/a]	$-0.0025 (\pm 0.0016)$	$-0.0037 (\pm 0.0045)$
$\gamma_{E \times B}$ [c_s/a]	$0.017 (\pm 0.016)$	$0.0015 (\pm 0.022)$	0.032	0.023
γ_P [c_s/a]	$0.16 (\pm 0.014)$	$0.015 (\pm 0.22)$
q	2.78	2.83
s	2.74	2.48

GYRO. Also, ν_{ei} is the electron-ion collision frequency, ω_o is the $E \times B$ toroidal rotation frequency, $\gamma_{E \times B}$ is the $E \times B$ shearing rate, and γ_P is a rotation shearing rate. q is the safety factor, and s is the magnetic shear defined as $s = r/q |dq/dr|$. Due to the low β values of plasmas used in this study ($\beta_t < 1\%$), it is expected that electromagnetic effects are negligible. Thus, only electrostatic simulations were performed. A realistic plasma shape is considered in the simulations through the Miller type equilibrium model,³⁸ based on the equilibrium information obtained from TRANSP. Electron collisions are modeled by using pitch angle scattering, and ion-ion collisions are not included in the simulations. Gyrokinetic ions and drift-kinetic electrons are used. One impurity species (Boron, B) is used with the estimated main ion fraction (n_D/n_e). It was assumed that the main ion density profile has the same radial gradient as the electron density profile, but with the different amplitude, determined by the main ion fraction. Although impurities can affect the main ion density gradient, we assumed that the main ion density gradient was not changed even when including impurities.

The nonlinear simulations include only ion scale turbulence $k_y \rho_s \lesssim 1.7$. Toroidal grid spacing is $\Delta n = 12$ with between 30 and 32 toroidal modes. The domain size was set to $L_x \sim 130 \rho_s$ by $L_y \sim 110 \rho_s$ with a radial grid spacing $\Delta x/\rho_s \sim 0.25$ for both the LOC and SOC plasmas. In velocity space, 128 grid points were set with 8 energies, 8 pitch angles, and 2 signs of velocity. All simulated quantities in this study were averaged in the stationary time period for more than $300[a/c_s]$, where the spatially averaged ion heat flux, Q_i , electron heat flux, Q_e , and potential fluctuations of

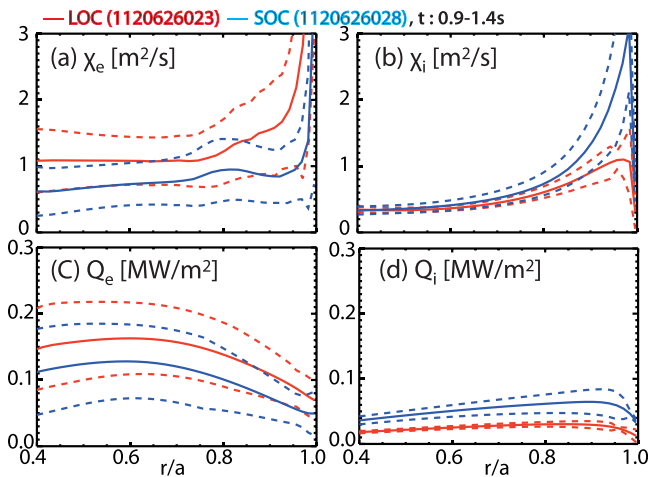


FIG. 4. Heat diffusivity and flux for LOC/SOC plasmas (red: LOC discharge, blue: SOC discharge) (a) Electron heat diffusivity (χ_e [m^2/s]), (b) ion heat diffusivity (χ_i [m^2/s]), (c) electron heat flux (Q_e [MW/m^2]), and (d) ion heat flux (Q_i [MW/m^2]). The solid line shows the experimental value and the dotted line indicates the uncertainty.

each toroidal modes are saturated. The uncertainties on the simulation outputs, which are spatially averaged fluctuating functions of time only, are estimated from the standard deviation of the mean values from $50 a/c_s$ subwindows in the stationary time period to average over the inherent variability due to turbulence.

Normally in validation studies, “base case” simulations are performed using the experimental profiles as input, without making any changes.^{3,39} However, we found that the nonlinear simulations in the outer core region of Ohmic L-mode plasmas at C-Mod are extremely challenging. If we just used the experimental inputs with no modifications, it was not possible to produce a well-resolved simulation without using unrealistically large box sizes (e.g., more than half the plasma minor radius). Instead, to develop the “base case” simulations, it was necessary to modify the $E \times B$ shearing rate in both the LOC and SOC plasmas and the density gradient in the SOC plasma. Table I lists the experimental values as well as the “base case” inputs for the GYRO simulations. To ensure the reliability of the results, we performed a series of convergence tests in simulation box size, the maximum simulated k , radial grid spacing, velocity space, and energy. These tests typically involved increasing the resolutions by approximately 50% in each dimension. It was found that these numerical variations did not change the simulated heat fluxes outside of diagnosed uncertainties. More details of the development of the “base case” simulations, including comparison with global GYRO simulations and discussion of the many convergence studies done, are found in Ref. 26.

For the SOC simulation, the eventual “base case” is a well-resolved run with reasonable domain size (L_x : $130.9\rho_s$, L_y : $114.3\rho_s$) where both the $E \times B$ shearing rate and the

normalized electron density scale length were increased by the 1-sigma error bars from Table I values. The SOC “base case” values are $\gamma_{E \times B} = 0.023[c_s/a]$ and $a/L_n = 1.87$. The value of a/L_{Ti} was kept at the experimental value ($a/L_{Ti} = 5.86$) for the SOC “base case”. Similarly, for the LOC simulation “base case,” a well-resolved run with reasonable domain size (L_x : $130.8\rho_s$, L_y : $107.1\rho_s$) was obtained. In this case, only the $E \times B$ shearing rate was increased by the 1-sigma error bar ($\gamma_{E \times B} = 0.032[c_s/a]$) from Table I. Again, the value of a/L_{Ti} was kept at the experimental value ($a/L_{Ti} = 5.54$) for the LOC “base case.”

IV. COMPARISON BETWEEN EXPERIMENT AND NONLINEAR GYROKINETIC SIMULATIONS

In this section, we describe comparisons between experimental fluctuation measurements and transport values from the outer core region ($r/a \sim 0.85$) with the local, nonlinear GYRO simulations described in Section III. We refer to a simulation as the “base case” when the input a/L_{Ti} value used is the experimental value from Table I (but the $E \times B$ shear and a/L_n values may have been changed). The simulations will be labeled “ion-heat flux matched” if the experimental ion heat flux has been matched by increasing only a/L_{Ti} by the 1-sigma experimental error.

The GYRO heat flux results from “base case” runs ($a/L_{Ti} \simeq 5.5$ in LOC, $a/L_{Ti} \simeq 5.8$ in SOC) and “ion-heat flux matched” runs ($a/L_{Ti} \simeq 6.3$ in LOC and $a/L_{Ti} \simeq 6.8$ in SOC) are compared in Figure 5 with each other and with the experimental power balance levels. In Figure 5 the solid black line is the power balance heat flux value and the horizontal dashed lines represent ± 1 sigma error bars on the power balance

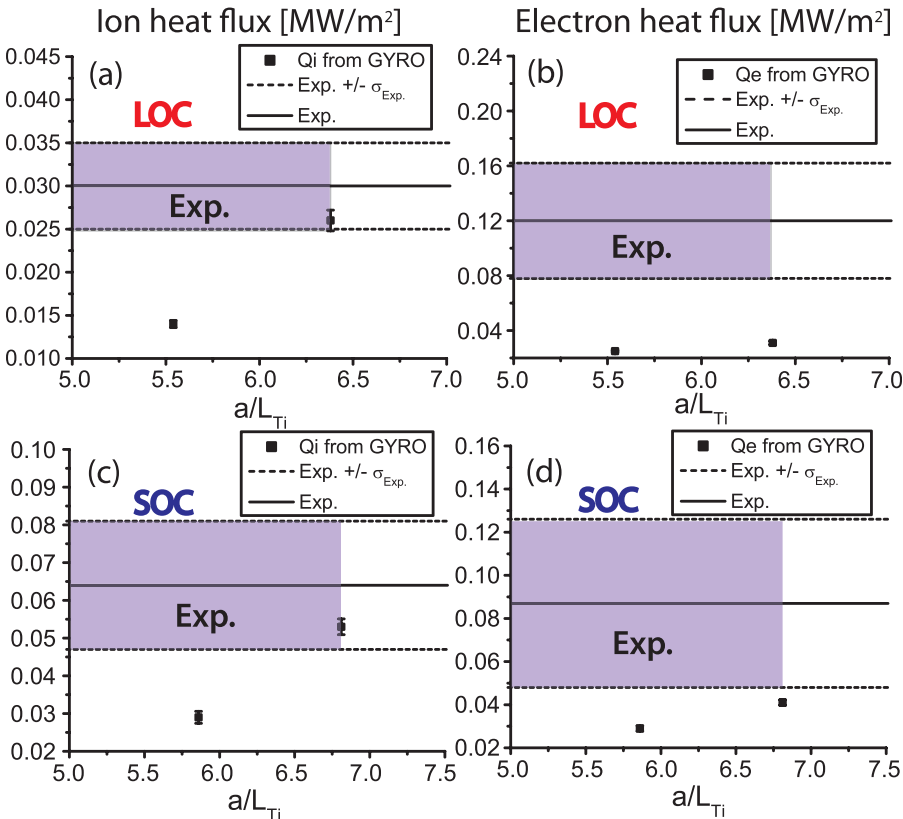


FIG. 5. Comparison of simulated heat fluxes from the “base case” runs ($a/L_{Ti} \simeq 5.5$ in LOC, $a/L_{Ti} \simeq 5.8$ in SOC) and “ion-heat flux matched” runs ($a/L_{Ti} \simeq 6.3$ in LOC, $a/L_{Ti} \simeq 6.8$ in SOC) with the experimental heat fluxes from power balance analysis (Section III describes the set-up for these simulations). The shaded region indicates the experimental region, formed by the uncertainties in the experimental heat fluxes and a/L_{Ti} . (a) Ion heat flux, Q_i [MW/m²] in the LOC plasma, (b) electron heat flux, Q_e [MW/m²] in the LOC plasma, (c) Q_i [MW/m²] in the SOC plasma, and (d) Q_e [MW/m²] in the SOC plasma.

values. In the base case, we found that the “base case” nonlinear simulations under-predicted ion heat flux Q_i and electron heat flux Q_e compared to power balance analysis in both LOC and SOC discharges. In the “ion-heat flux matched” simulations, it was possible to match Q_i by increasing a/L_{Ti} by the 1-sigma error bar, but the electron heat flux, Q_e is still substantially under-predicted in the LOC plasma. In the SOC plasma, the simulated electron heat flux is closer to the experimental level compared to the LOC plasma, but still under-predicted. The experimental trend from power balance showed an increase of Q_i and the decrease of Q_e across the LOC/SOC transition. The pair of “ion-heat flux matched” simulations show that both Q_i and Q_e increase going from LOC to SOC. The trend in Q_i is consistent with experiment, but the increase of Q_e is not, although we note that the change in Q_e is still within the range of experimental uncertainty.

For comparisons between CECE fluctuation measurements and GYRO results, the “ion-heat flux matched” simulations are used. In order to compare simulated electron temperature fluctuations directly with the CECE measurements, we need a computational model which can convert the simulated “raw” outputs into simulated diagnostic signals by considering the experimental limits on spatial resolution and Doppler-shift effects. This computational model is called a synthetic diagnostic.^{3,40} In this study, we modified an existing synthetic diagnostic model for the CECE diagnostic in DIII-D³ for use in C-Mod. The synthetic model used in this study is described in Ref. 26.

The same signal analysis process was applied to both the synthetic (simulation data) and measured fluctuation time series (experimental data). Figure 6(a) shows the measured temperature fluctuation level compared with the GYRO synthetic fluctuation level. The cross-power spectrum is integrated over the frequency range 0–170 kHz to obtain the fluctuation level, since 170 kHz is the highest frequency where we observed turbulent fluctuations in both the LOC and SOC discharges. The fluctuation levels agree within error bars with experiment in both LOC and SOC. But there is no difference between LOC and SOC outside of error bars for the synthetic fluctuation levels (due to the estimated uncertainties on the simulation results). The synthetic cross-power spectra compared with experimental cross-power spectra are shown in Figure 6(b) for the LOC plasma and 6(c) for the SOC plasma. While the amplitude of the fluctuations agree within error bars, the shapes of the simulated spectra do not agree with experiment. The GYRO predicted spectra are more narrow in frequency (less Doppler shifted) than the experimental spectra. In these simulations, the E_r value estimated from TRANSP (~ -1 kV/m) was used. As will be explored later, the discrepancy in the spectral shape can be resolved by using $E_r \sim 9$ kV/m, which required an additional input parameter change (other than just a/L_{Ti}), so the discussion is deferred to Section V.

V. SENSITIVITY OF SIMULATION RESULTS TO CHANGES IN THE INPUT PARAMETERS

In Section IV, we showed by increasing the input a/L_{Ti} by the 1-sigma experimental error bar that local, nonlinear

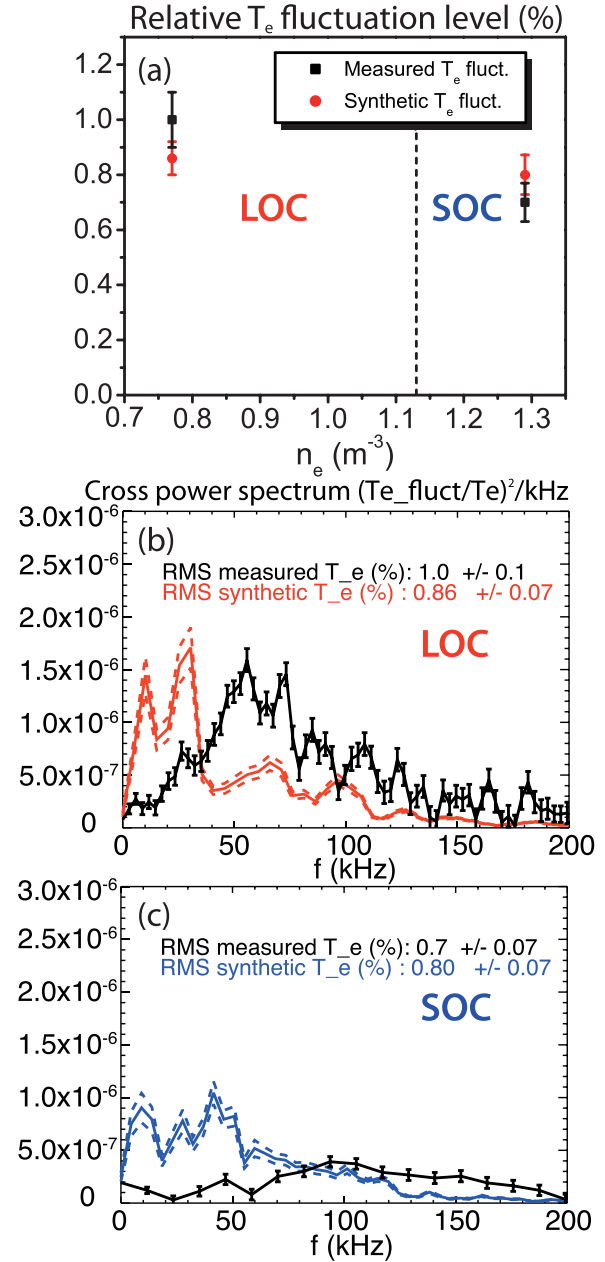


FIG. 6. Comparison of synthetic \tilde{T}_e/T_e fluctuations with the measurements in the LOC and SOC plasmas (a) relative \tilde{T}_e/T_e fluctuation level in both the LOC/SOC plasmas, (b) cross power spectrum in the LOC, and (c) cross power spectrum in the SOC. The dotted lines in (b) and (c) indicate the error in the synthetic spectrum.

long-wavelength electrostatic GYRO simulations can match both the experimental levels of ion heat flux and electron temperature fluctuations within experimental error bars. In these same simulations, the electron heat flux is below the experimental values and the synthetic spectra were narrower than experiment. Possible reasons for these discrepancies are investigated in this section.

A. Sensitivity of ion heat flux and electron temperature fluctuation levels

For these scans, we change many different input parameters within their uncertainties, that is, $X \pm \sigma_X$ was used for

the sensitivity analysis, where X is a certain input parameter and σ_X is the 1-sigma value of the experimental uncertainty.

Figure 7 shows the fractional changes in Q_i and synthetic \tilde{T}_e/T_e fluctuation levels with the changes in each input parameter. From Figs. 7(a) and 7(b), we first notice that a/L_{T_i} and a/L_{T_e} are the most sensitive parameters for Q_i in both discharges. Increasing a/L_{T_i} by its uncertainty ($\sim 15\%$) results in an approximately 80% increase in Q_i . The sharp increase in Q_i with the increase of a/L_{T_i} will indicate that ITG mode is important in these simulations. It is also shown that Q_i increases with other ITG favorable changes such as increasing n_D/n_e and a/L_n .

Unlike a/L_{T_i} , the decrease of a/L_{T_e} by its uncertainty ($\sim 20\%$ – 25%) increases Q_i by more than 50%. The increase of a/L_{T_e} also affects Q_i significantly by decreasing it by more than 20%, although the variation in Q_i is smaller than the decrease of a/L_{T_e} . Increasing the electron-ion collision frequency, ν_{ei} , will decrease the activity of trapped electrons, that is, the non-adiabatic electron response. Since non-adiabatic electrons destabilize the ITG mode as well as TEM, although ITG mode can be destabilized without non-adiabatic electrons, it is hard to connect the changes in Q_i with ν_{ei} to a specific turbulence mode, either ITG or TEM. It will be more appropriate to leave it as the effect of the response of non-adiabatic electrons rather than a certain turbulence mode. It is shown that Q_i decreases with the increase in ν_{ei} (or the reduction of non-adiabatic electron response) in both LOC and SOC discharges. However, Q_i changes within 20% by increasing/decreasing ν_{ei} by its uncertainty ($\sim 20\%$). This 20% variation indicates that Q_i is less sensitive to ν_{ei} than to gradient scale lengths. In the LOC discharge, dilution or main ion fraction, n_D/n_e also changes Q_i by more than 20%, which is consistent with the previous study in C-Mod.^{9,41}

Figures 7(c) and 7(d) show the changes in synthetic \tilde{T}_e/T_e fluctuation levels with input parameters. Similar to Q_i , synthetic fluctuation levels increase with ITG favorable changes such as the increase of a/L_{T_i} and n_D/n_e and the decrease of a/L_n . It is noteworthy that the largest variation in synthetic \tilde{T}_e/T_e fluctuation levels is obtained from the decrease of a/L_n by its uncertainty ($\sim 40\%$), not from the increase of a/L_{T_i} . Even the increase of n_D/n_e changes the synthetic \tilde{T}_e/T_e fluctuation levels by more than the increase of a/L_{T_i} in the LOC discharge. The dependency of synthetic \tilde{T}_e/T_e fluctuation levels on a/L_{T_e} is also interesting. The decrease in a/L_{T_e} increases the synthetic level in both LOC and SOC discharges. This can be interpreted as the result of a more destabilized ITG mode, consistent with the sensitivity of Q_i . However, the increase in a/L_{T_e} also increases the synthetic \tilde{T}_e/T_e fluctuation level. More destabilized TEM turbulence due to the increase of a/L_{T_e} may cause the increase of \tilde{T}_e/T_e fluctuation level. This indicates that synthetic \tilde{T}_e/T_e fluctuation levels respond to both ITG and TEM relevant changes. Thus, we should be careful when connecting the changes in \tilde{T}_e/T_e fluctuations with the changes in the specific turbulence mode. Dependency of synthetic \tilde{T}_e/T_e fluctuations on ν_{ei} is similar to the observation in Q_i , but synthetic level increases not only with the increase in ν_{ei} but also with its decrease in the SOC discharge. An approximately 3% increase in synthetic \tilde{T}_e/T_e fluctuation levels with the increase of ν_{ei} might not be meaningful. If the ν_{ei} value in the SOC discharge is already high enough to suppress most of the response of non-adiabatic electrons, then the synthetic \tilde{T}_e/T_e fluctuation levels with the ν_{ei} above this level will be saturated and fluctuate within the uncertainty. If this is the case, we may need to think of the 3% increase of the fluctuation level with the increase in ν_{ei} as the saturation rather than the increase. In order to verify this possibility, a

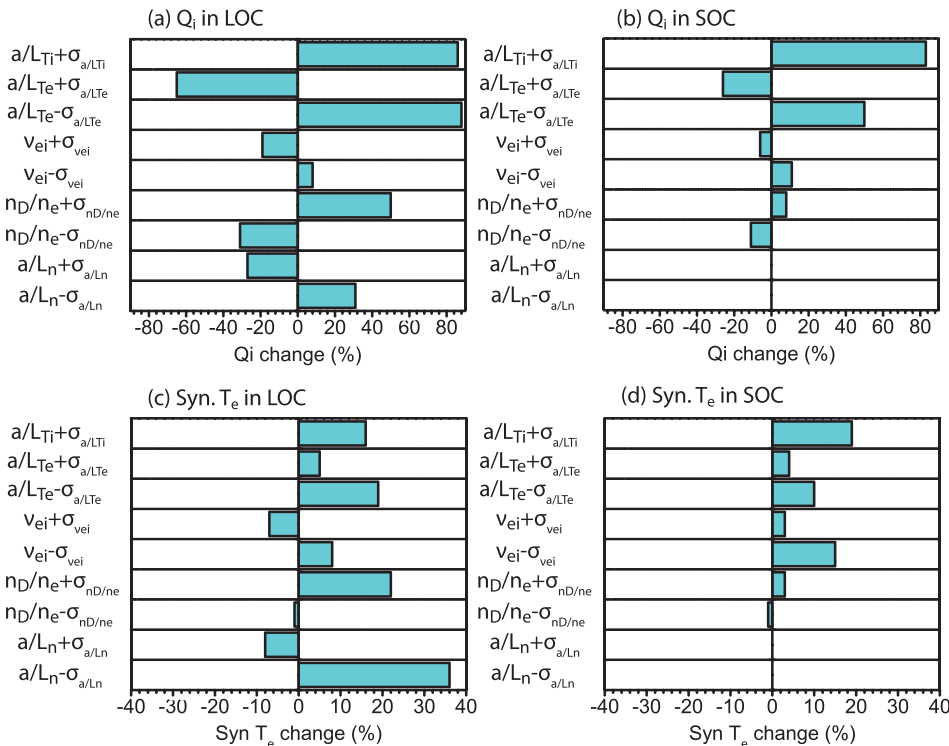


FIG. 7. Fractional changes in the simulated ion heat flux and synthetic electron temperature fluctuation level with input parameter changes at the CECE measurement position ($r/a \sim 0.85$) for the LOC and SOC discharges (shot: 1120626023 (LOC), 1120626028 (SOC)). (a) Ion heat flux, Q_i , in the LOC discharge, (b) Q_i in the SOC discharge, (c) synthetic \tilde{T}_e/T_e fluctuation level in the LOC discharge, and (d) synthetic \tilde{T}_e/T_e fluctuation level in the SOC discharge. a/L_n was fixed in the SOC discharge, then the fractional change due to a/L_n was represented as zero in the SOC discharge.

run with higher ν_{ei} outside experimental uncertainty would likely be required.

B. Sensitivity of electron heat flux level

The under-prediction of the electron heat flux by the long wavelength simulations is found to be robust and cannot be resolved by changing experimental inputs within error bars. Figure 8(a) shows that the highest Q_e values obtained from the sensitivity analysis runs are still under-predicted from the experimental level in both LOC and SOC discharges.

The variations of Q_e with the changes in input parameters are shown in Figs. 8(b) and 8(c). The increase in a/L_{Ti} causes the largest variation in Q_e in both discharges. We also note that there was no change in Q_e with the increase of a/L_{Te} in the SOC discharge, while Q_e increases about 15% with the increase of a/L_{Te} in the LOC discharge. Since the increase of a/L_{Te} is favorable for TEM, this may indicate that TEM is more important in the LOC discharge than the SOC discharge. We also note that the variation of Q_e with a/L_{Te} changes is less than 20%. Thus, the variations of Q_e with a/L_{Te} are smaller than the variations with a/L_{Ti} .

In the LOC discharge, Q_e is sensitive to n_D/n_e and the increase of ν_{ei} . In the same discharge, Q_e increases about 10% with the decrease of a/L_n in the LOC discharge, although synthetic \tilde{T}_e/T_e fluctuation levels increase by about 40%. In the SOC discharge, Q_e does not vary significantly (less than 10%) with input parameter changes except for the increase of a/L_{Ti} , while synthetic \tilde{T}_e/T_e fluctuations are sensitive to the decrease of ν_{ei} as well as a/L_{Ti} in the same discharge. Q_e is a function of three fluctuating quantities (potential fluctuations, n_e and T_e fluctuations) and their phase relations. Synthetic \tilde{T}_e/T_e fluctuation level is a function of T_e fluctuations and can be also affected by n_e fluctuations and the phase between T_e and n_e fluctuations if optical depth is not high enough. Thus, the sensitivity of Q_e to the changes in the inputs is not necessarily identical to the sensitivity of synthetic T_e fluctuations. This is because the synthetic \tilde{T}_e/T_e fluctuations are limited to low k_y turbulence, $k_y\rho_s < 0.3$, whereas the simulated electron heat flux comes from all simulated $k_y\rho_s$ values. Further analysis of the impact of electron temperature gradient (ETG) scale turbulence on the electron heat flux is likely required to investigate the physics behind different sensitivities of Q_e and synthetic \tilde{T}_e/T_e fluctuations.

In Sections VA and VB, we varied one variable at a time to see the dependence of the simulated heat transport and synthetic T_e fluctuations on each parameter. However, it will be also interesting to see how the simulated transport and fluctuations are varied with the coupled changes such as increase in both a/L_{Te} and a/L_{Ti} simultaneously or increase in a/L_{Te} with decrease in a/L_{Ti} and see whether the sensitivity on each parameter observed in this sensitivity study will be just added up in the run with a coupled changes or not. These interesting runs should be performed in the future.

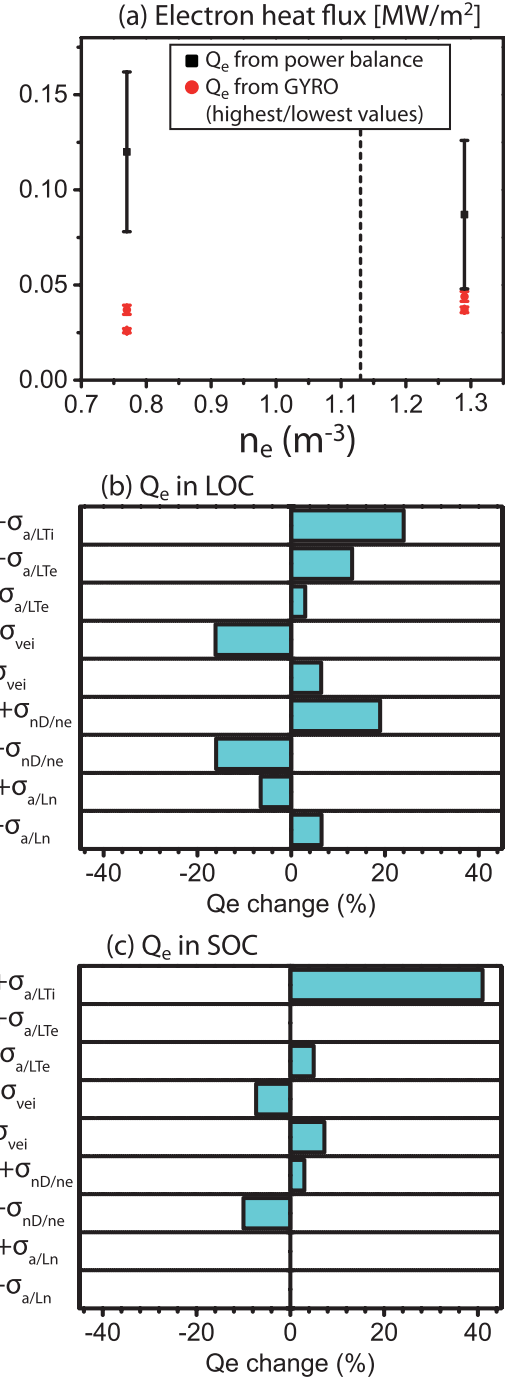


FIG. 8. (a) Comparison of the highest and lowest values of simulated electron heat flux obtained from the sensitivity analysis for the LOC/SOC discharges at the CECE measurement position ($r/a \sim 0.85$) (shot: 1120626023 (LOC), 1120626028 (SOC)) with the experiments. Fractional changes in the simulated electron heat flux with input parameter changes in the same sensitivity analysis for (b) the LOC discharge and (c) the SOC discharge. a/L_n was fixed in the SOC discharge, and the fractional change due to a/L_n was represented as zero in the SOC discharge.

C. Shape of the experimental temperature fluctuation frequency spectra

We first checked whether or not the ion-heat flux matched GYRO simulations could reproduce the measured \tilde{T}_e/T_e fluctuation spectral shape by varying the rotation frequency, ω_o within its uncertainty. In these simulations, GYRO uses the rotation frequency calculated from the radial

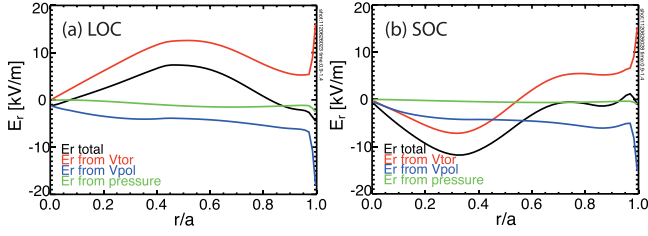


FIG. 9. Total E_r value with the contribution of each component (toroidal velocity, V_{tor} , poloidal velocity, V_{pol} , and pressure gradient) estimated from TRANSP in (a) the LOC discharge and (b) the SOC discharge.

electric field, E_r . This E_r value is estimated from TRANSP using the force balance equation as follows:⁴²

$$E_r = \frac{1}{n_i Z_i e} \frac{dP_i}{dr} - V_{p,i} B_t + V_{t,i} B_p, \quad (1)$$

where n_i , Z_i , and P_i are the density, charge, and pressure of the ion used in the E_r calculation. $V_{p,i}$ and $V_{t,i}$ are the poloidal and toroidal velocities of the ion, respectively, and B_t and B_p are the toroidal and poloidal magnetic field, respectively. TRANSP uses the experimental toroidal velocity and pressure gradient to estimate the first and second terms, and a neoclassical calculation is used to estimate the poloidal velocity through the NCLASS module⁴³ for the third term in Eq. (1).

We found that the neoclassical rotation values in both toroidal and poloidal directions for LOC and SOC plasmas are not always consistent with measurements, which indicates that rotation can be induced by other mechanisms, such as turbulence.^{44–46} Applying the calculated neoclassical poloidal velocity can be an issue, since the contribution of the poloidal velocity term to total E_r value is not negligible. As shown in Fig. 9, the contribution of the poloidal velocity term is comparable to the contribution of the toroidal velocity term at $r/a \sim 0.85$, and the pressure gradient term is small compared to the other two terms at this location (in contrast

to the pedestal region at C-Mod, where the diamagnetic term is usually dominant^{47,48}). We also see that the sign of the toroidal and poloidal velocity terms is opposite. Then, canceling out two terms results in a small E_r value near to zero. In this situation, if the real poloidal velocity has the opposite sign to the estimated neoclassical value, it will change the estimated experimental E_r value significantly. It is therefore possible that the TRANSP calculated neoclassical rotation profile was not consistent with the experiments, and is resulting in a GYRO predicted CECE spectrum that is narrower than the measured.

In order to check this possibility, we used the edge charge exchange recombination spectroscopy (CXRS) diagnostic to estimate the E_r value with the measured toroidal/poloidal velocity and pressure gradient. We note that in the past analysis of these discharges¹³ the x-ray spectroscopy data (available only inside $r/a < 0.80$) was used to constrain the experimental rotation profiles. Here, we have improved the analysis by combining the x-ray spectroscopy data ($r/a < 0.80$) with the CXRS data ($r/a > 0.80$), in order to better constrain the E_r profile at the CECE measurement location. The measured E_r by CXRS at $r/a \sim 0.85$ is 3 ± 12 kV/m for both the LOC and SOC discharges. The estimated E_r value from TRANSP is ~ -1 kV/m, which is consistent with the measurements within the large uncertainty. For the comparison of fluctuation spectra, we used the Q_i matched run for the LOC discharge and the low n_D/n_e run ($n_D/n_e = (n_D/n_e)_{exp} - \sigma_{nD/n_e}$) for the SOC discharge. It was found that the synthetic spectral shape is similar to the measured spectrum over a broad frequency range when $E_r \sim 9$ kV/m, which is within the uncertainty of the measured E_r value, as shown in Fig. 10. Given that the CXRS measurements constrain E_r to be near zero at these measurement locations ($E_r = 3 \pm 12$ kV/m) and since the simulations are being run to match the ion heat flux, the choice of $\mathbf{E} \times \mathbf{B}$ shear used in the simulations should not alter the calculated momentum flux, which should be close to zero in the simulations (or

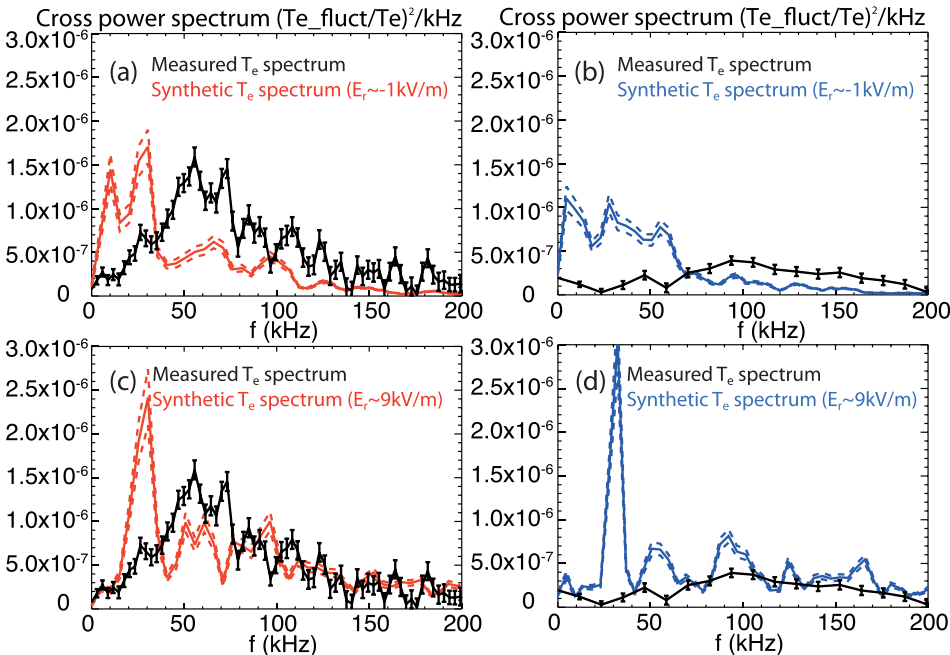


FIG. 10. Comparison of the synthetic \tilde{T}_e/T_e fluctuation spectrum with the measured spectrum when the E_r value estimated from TRANSP (~ -1 kV/m) was used for (a) the LOC discharge and (b) the SOC discharge. The synthetic spectral with $E_r \sim 9$ kV/m for (c) the LOC discharge and (d) the SOC discharge is also compared with the measurements.

more accurately, the sum of turbulent and neoclassical momentum fluxes is zero). For these simulations, indeed we find that the gyroBohm normalized ion momentum fluxes (including the impurity) are small (~ 4 – 6) in both LOC and SOC plasmas, considering the gyroBohm normalized ion heat fluxes (including the impurity) are ~ 20 – 40 . The gyroBohm unit momentum and heat fluxes are defined as $\Pi_{gb} = n_e a T_e (\rho_s/a)^2$ and $Q_{gb} = n_e T_e c_s (\rho_s/a)^2$, respectively.

However, when the simulations were run with $E_r \sim 9$ kV/m, we found a new feature in the simulated synthetic CECE spectra—a narrow peak near 30 kHz in the synthetic spectra in both LOC and SOC discharges. This narrow peak is shown in Figure 10, panels (c) and (d). In several other experiments^{49,50} coherent or quasi-coherent peaks are observed in measured density fluctuations and these peaks are reproduced by simulations. In these other works, the simulated coherent peak is interpreted as arising from real physical fluctuations, specifically density gradient TEM⁴⁹ or temperature gradient TEM.⁵⁰ But in our experiments, we did not observe any coherent peak in the measured temperature fluctuations, so we suspected that the peak seen in the simulations was related to a numerical issue.

Often, a peak in the heat flux or fluctuations in a nonlinear simulation arises at the smallest simulated k_y value due to inadequate resolution or box-size. But in this case, the peak occurs at a higher value of k_y than the smallest in the box, so it does not appear to be caused by such a resolution issue. Several simulations for box-size scans and radial grid scans, not shown here, but described in Ref. 26, confirmed this, as the peak was still present across those scans.

The high collisionality in both the LOC and SOC plasmas at these outer core radial locations ($r/a \sim 0.85$) could be causing accuracy issues when using lower order radial basis function (RBF) expansions.⁵¹ Indeed, we found that the order of the radial basis function used to evaluate the collision operator⁵² does indeed affect the coherent peak seen in the simulated spectrum. In our simulations, we can eliminate

the coherent peak by increasing the order of the radial basis function (RBF), by using the GYRO variable name ORD_RBF, from 3 (default, used in the base case and ion-heat flux matched runs) to 5 (which is recommended to use when the collision frequency is near unity). In the SOC plasma at the simulated radius, the collision frequency, $\nu_{ei} = 1.28$ (Table I), and in the LOC plasma, $\nu_{ei} = 0.56$ (Table I). Interestingly, the increase in the order of the radial basis function strongly mitigates the coherent peak in the simulated spectrum in both plasmas. Authors also note that the changes in heat fluxes with the order of the radial basis function are within their uncertainties, indicating the sensitivity analyses with 3rd-order RBFs in this study are still valid.

Figure 11 shows the synthetic spectra in the LOC/SOC discharges with the same E_r value as ~ 9 kV/m but with different values of the order for the radial basis function, where 3rd-order RBFs used in Figures 11(a) and 11(c) and 5th-order RBFs used in Figures 11(b) and 11(d). It is shown that increasing the order of the radial basis function suppresses the peak significantly, and that the synthetic spectrum with 5th-order RBFs becomes more similar to the measured spectrum. These simulations show that GYRO can reproduce the measured spectral shape in a broad frequency range in both LOC and SOC discharges within the uncertainty of the measured E_r values by CXRS, which implies that GYRO predicted the correct \tilde{T}_e/T_e fluctuation spectrum in k space. This also suggests that the inaccurate estimation of poloidal velocity from neoclassical calculation is the reason for the narrower synthetic \tilde{T}_e/T_e fluctuation spectra compared to the experiments. However, we should note that the uncertainty in the E_r measurements for the LOC/SOC discharge is about 400%. In the future, we need a dedicated experiment for more accurate E_r measurements in Ohmic discharges to see whether or not the neoclassical poloidal velocity used in GYRO is responsible for the discrepancy of the \tilde{T}_e/T_e fluctuation spectral shape.

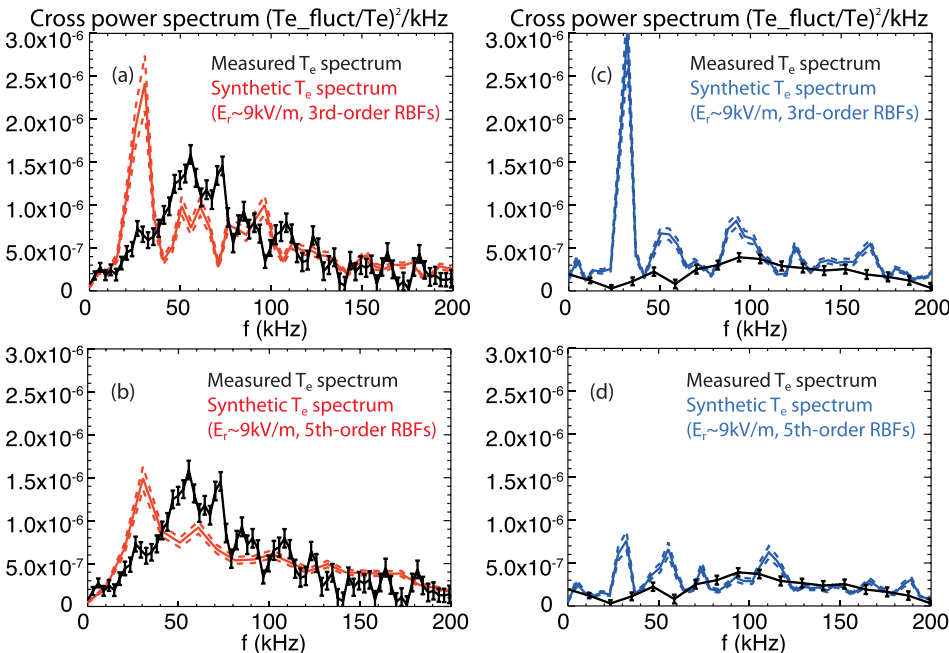


FIG. 11. Comparison of the synthetic \tilde{T}_e/T_e fluctuation spectrum with the measured spectrum with $E_r \sim 9$ kV/m using the simulations with different values of the order of the radial basis function (GYRO variable ORD_RBF). (a) Result from the LOC plasma simulation with the 3rd-order RBFs, (b) result from the LOC plasma simulation with the 5th-order RBFs, (c) result from the SOC plasma simulation with the 3rd-order RBFs, and (d) result from the SOC plasma simulation with the 5th-order RBFs.

VI. INVESTIGATION OF THE ITG/TEM HYPOTHESIS FOR THE LOC/SOC PLASMAS

In this section, we discuss the results from nonlinear simulations in the context of LOC/SOC hypothesis, to determine if the nonlinear simulations provide any evidence that TEM turbulence is more active in the LOC plasma and ITG turbulence is more active in the SOC plasma.

First, we compare the eigenvalue linear stability analysis shown previously (Figure 3) when the experimental values were used as inputs to the linear stability analysis using the “ion-heat flux matched” simulation inputs. Figure 12 shows the changes in both dominant and sub-dominant linear unstable modes between two discharges, using “ion-heat flux matched” simulation inputs. In both discharges, three or four unstable ion modes exist, and their growth rates are comparable between the two discharges. The SOC discharge has two unstable electron modes in $k_y \rho_s \leq 0.3$, while the LOC

discharge has one unstable electron mode in the CECE relevant region. However, the growth rate of the sub-dominant electron mode in $k_y \rho_s \leq 0.3$ in the SOC discharge is not significant, less than the $E \times B$ shearing rate used in this simulation (~ 15 kHz), and also less than half of the growth rate of the dominant electron mode. The growth rates of the dominant electron mode in $k_y \rho_s \leq 0.3$ are comparable between the LOC and SOC discharges. In $k_y \rho_s > 0.3$, the electron mode in the LOC discharge has the higher growth rate compared to the SOC discharge, consistent with the linear stability analysis results in Section II. Similar to the linear stability analysis results using experimental values as input, the linear stability analysis performed using the “ion-heat flux matched” simulation inputs shows no clear evidence of a transition from TEM to ITG turbulence across the LOC/SOC transition, but TEM turbulence in $k_y \rho_s > 0.3$ is more unstable in the LOC discharge compared to the SOC.

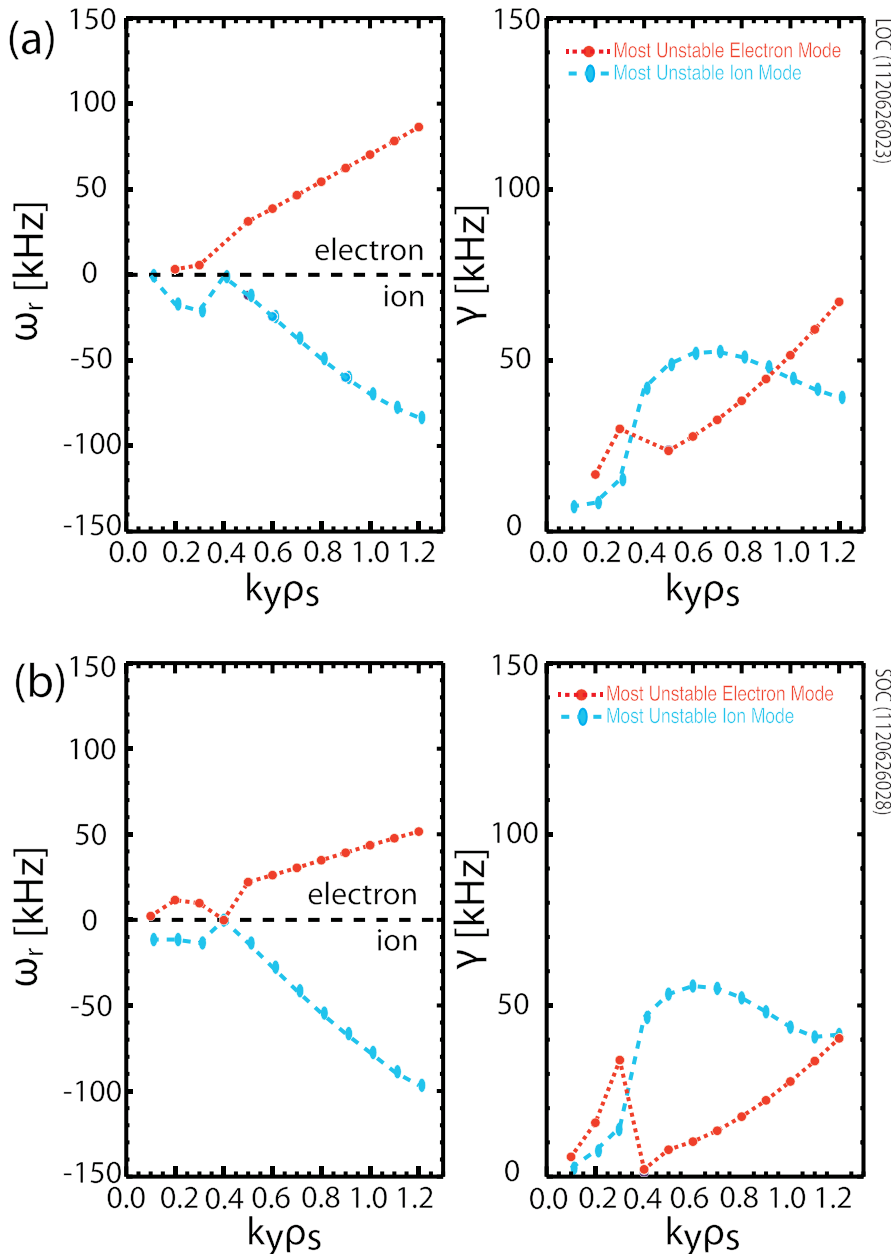


FIG. 12. Linear stability analysis using eigenvalue solver with the input parameters used in the Q_i matched simulations for (a) the LOC discharge (shot 1120626023) and (b) the SOC discharge. Red-circle, dotted line: most unstable electron mode, blue-oval, dashed line: most unstable ion mode.

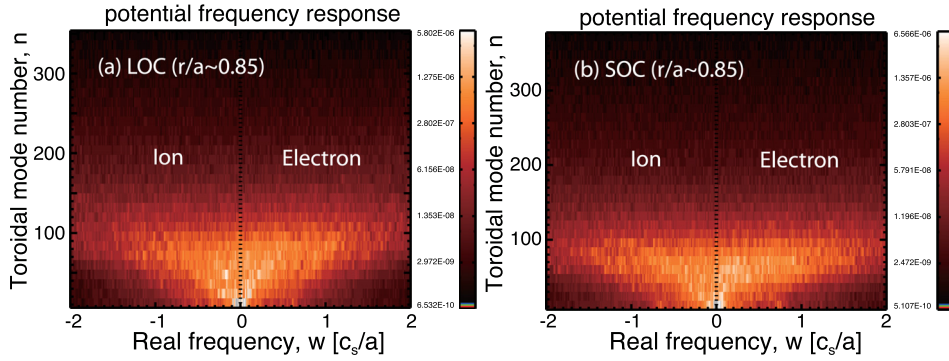


FIG. 13. Power spectrum of simulated potential fluctuations on the midplane from Q_i matched simulations at the CECE measurement position for (a) the LOC discharge (shot:1120626023) and (b) the SOC discharge (shot: 1120626028) with experimental input values. The simulated potential fluctuations are averaged radially.

Second, we examined the results from the ion-heat flux matched nonlinear simulations. The direction of propagation of the turbulence in the simulation can be seen in the plot of the power spectrum of fluctuations on the midplane per toroidal number, n , as shown in Figure 13. For both LOC and SOC discharges, there is no clear propagation direction, with the turbulence propagating in both the ion and electron diamagnetic drift directions (negative and positive real frequencies in GYRO, respectively). In addition, there is no difference in mode structure in the simulations. This result indicates that there are no changes in the dominant turbulence mode between the LOC and SOC discharges near the edge region.

Third, we looked to the results from the sensitivity scans discussed in Sections V A and V B. The sensitivity analysis showed that a/L_{Ti} is one of the strongest knobs to change the simulated levels of Q_i , Q_e and synthetic \tilde{T}_e/T_e fluctuation levels in both LOC and SOC discharges. a/L_{Te} is also important for Q_i and synthetic \tilde{T}_e/T_e fluctuation levels, while Q_e varies less than 20% with the changes in a/L_{Te} in both discharges. However, it is also noteworthy that Q_e in the LOC discharge is more sensitive to a/L_{Te} compared to the SOC discharge, suggesting that TEM is more important in the LOC discharge. These results may indicate that the contribution of ITG to the heat transport is larger than that of TEM in both discharges although TEM is not ignorable in these simulations. It was observed that n_D/n_e is important in the LOC discharge, consistent with previous studies.^{9,41} a/L_n is also an important parameter for Q_i and synthetic \tilde{T}_e/T_e fluctuations in the LOC discharge. Although variations of ν_{ei} by its uncertainty do not result in significant changes in synthetic \tilde{T}_e/T_e fluctuation levels, the consistent trend of synthetic \tilde{T}_e/T_e fluctuation levels with ν_{ei} in the experiments was observed, while the trend of \tilde{T}_e/T_e fluctuation levels with n_D/n_e was opposite to the experiments.

So far, we have shown that there is no dominant turbulence mode change from TEM to ITG across the LOC/SOC transition. However, it is true that ion heat transport is enhanced significantly in the SOC discharge compared to the electron heat transport and that ion heat flux is larger than electron heat flux in the SOC discharge, while it is opposite in the LOC discharge as shown in Table II. Table II shows the simulated heat flux values and RMS fluctuation levels on the mid-plane output from the ion-heat flux matched runs for the LOC and SOC discharges. In order to understand the changes in heat transport between the LOC and SOC discharges, we investigated the differences in other turbulence

parameters between the LOC/SOC discharges, looking at parameters that are not currently measured such as potential and ion temperature fluctuations. There is more than a 30% increase of potential fluctuations in the SOC discharge compared to the LOC discharge. Ion temperature fluctuations also increase in the SOC discharge about 10%–20% compared to the LOC discharge, while electron temperature fluctuations decrease about 15% in the SOC discharge. Both electron and ion density fluctuations vary within 10% between the LOC and SOC plasmas. The increase of potential and ion temperature fluctuations can be linked to the higher ion heat flux in the SOC discharge. The increase of electron heat flux can also be explained by the increase of potential fluctuations. The decrease of electron temperature fluctuations may mitigate the increase of electron heat flux in the SOC discharge. We should note that potential and density fluctuations are within the uncertainty of the simulations. Nevertheless, the increases in potential and ion temperature fluctuations result in an increase in ion heat flux by a factor of 2. In addition, heat flux spectra on $k_y\rho_s$ were compared between the LOC/SOC discharges, as shown in Figure 14. We first note that ion heat flux is mainly come from $k_y\rho_s < 0.5$, and the main ion heat flux is increased in all $k_y\rho_s$ value in $k_y\rho_s < 0.5$. In the electron heat flux spectra, we can notice that the fraction of electron heat flux in $k_y\rho_s > 0.5$ in total electron heat flux is larger in the LOC discharge compared to the SOC discharge. The electron heat flux in $k_y\rho_s < 0.5$ in the SOC is larger than the electron heat flux in $k_y\rho_s < 0.5$ in the LOC. Interestingly, the electron heat flux in

TABLE II. The simulation results of the “ion heat flux matched case” for the LOC/SOC discharges at the CECE measurement position. Heat fluxes are averaged in space and time. Fluctuations are the values on the midplane and are averaged radially and in time. The uncertainties of midplane fluctuations and heat fluxes come from the standard deviation of the mean values from subwindows ($\Delta t = 50 [a/c_s]$, $\Delta r \sim 25\rho_s$), taking into account the auto-correlation time and length of the fluctuations.

	LOC	SOC
Q_i (MW/m ²)	0.026 (± 0.0012)	0.053 (± 0.0021)
Q_e (MW/m ²)	0.031 (± 0.0012)	0.041 (± 0.0013)
Syn. \tilde{T}_e/T_e (%)	0.86 (± 0.06)	0.80 (± 0.07)
$e\tilde{\phi}/T_e$ (%)	4.03 (± 0.57)	5.54 (± 1.32)
\tilde{n}_i/n_i (%)	1.97 (± 0.075)	1.84 (± 0.11)
\tilde{n}_e/n_e (%)	1.64 (± 0.074)	1.68 (± 0.10)
\tilde{T}_i/T_i (%)	3.62 (± 0.28)	4.07 (± 0.26)
\tilde{T}_e/T_e (%)	2.70 (± 0.12)	2.26 (± 0.10)

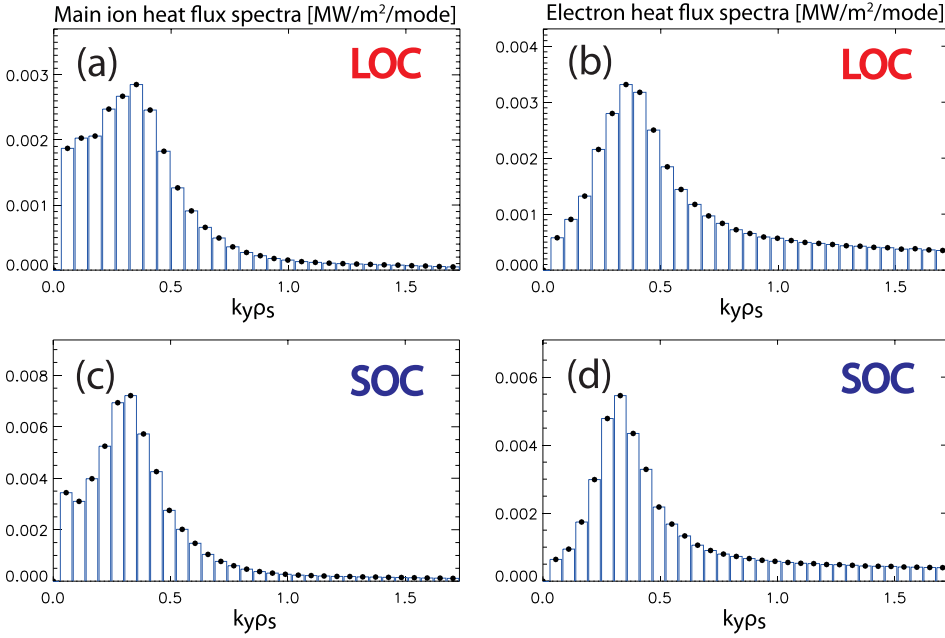


FIG. 14. Time averaged heat flux spectra on $k_y \rho_s$ in the “ion heat flux matched” runs (a) main ion heat flux spectrum in the LOC discharge (shot 1120626023) and (b) electron heat flux spectrum in the LOC discharge (c) main ion heat flux spectrum in the SOC discharge (shot 1120626028) and (d) electron heat flux spectrum in the SOC discharge.

$k_y \rho_s > 0.5$ in the SOC discharge is comparable to the LOC discharge. (Total electron heat flux in $k_y \rho_s > 0.5$ is about 0.014 MW/m^2 in both LOC and SOC discharges.) This can be considered as opposite compared to linear stability analysis, which shows the reduction of electron mode growth rate in $k_y \rho_s > 0.5$. However, if the conductive heat flux ($\sim n_e \tilde{T}_e \tilde{\phi}$) is significant or larger compared to the convective heat flux ($\sim T_e \tilde{n}_e \tilde{\phi}$) in the turbulent electron heat transport (electrostatic), it is expected that higher heat flux with higher density unless there is no dramatic turbulence change, e.g., turbulence change in L/H transition. Then, the same amount of heat flux with higher density may indicate the reduction of turbulence in this $k_y \rho_s$ range, which can be consistent with the linear stability analysis. It is also worth noting that electron heat flux is significantly under-predicted in these simulations. It is therefore not evident that these simulations describe well the electron heat transport changes across the LOC/SOC transition, as will be discussed in Section VII.

All these results can be summarized as follows: There is no dominant turbulence mode change from TEM to ITG between the LOC and SOC discharges in C-Mod. However, this does not mean that there is no change in turbulence between these two discharges. Linear stability analysis shows that electron mode turbulence in $k_y \rho_s > 0.3$ is more unstable in the LOC discharge compared to the SOC, and the sensitivity of Q_e on a/L_{Te} in the nonlinear simulations suggests that TEM is more important although both discharges have “mixed mode.” Thus, this study shows that TEM is relatively more important in the LOC discharge compared to the SOC discharge. However, it is not necessarily that dramatic linear transition between ITG and TEM across the LOC/SOC transition.

VII. IMPACT OF MISSING HIGH-K TURBULENCE ON THE ELECTRON HEAT FLUX LEVEL

So far, we have observed that GYRO can reproduce experimental ion heat flux levels, Q_i , \tilde{T}_e/T_e fluctuation

levels, and \tilde{T}_e/T_e fluctuation spectral shape by modifying input values within the uncertainty of the measurements. However, the electron heat flux, Q_e , is under-predicted in all simulations robustly. Since both Q_e and synthetic \tilde{T}_e/T_e fluctuations are related to electron transport, the disagreement with electron heat flux and agreement with temperature fluctuations appear incompatible. However, the measured \tilde{T}_e/T_e fluctuations come from low k_y , ion scale, turbulence ($k_y \rho_s < 0.3$), and the synthetic diagnostic takes this into account. In contrast, the GYRO simulated Q_e comes from only ion scale turbulence ($k_y \rho_s \lesssim 1.7$) included in the low-k simulations, while the experimental Q_e from power balance analysis can be caused by turbulence spanning the ion to electron scales. In Sections IV and V, we have shown agreement within the uncertainty in Q_i and synthetic \tilde{T}_e/T_e fluctuations, and the disagreements in Q_e with the experiments. In other words, the simulations agree with the experimental quantities that are predominantly linked to ion scale turbulence. This suggests that the small-scale electron temperature gradient (ETG) turbulence, that is not included in the simulations used in this study, could be primarily responsible for the disagreement in Q_e . According to a simple mixing length estimate, which shows diffusivity induced by turbulence which has a growth rate, γ , and wavenumber, k , $\chi \sim \gamma/k^2$, the contribution of electron scale turbulence to the transport will be ignorable due to its short wavelength. However, previous non-linear simulation works show that electron transport, above the estimated level from a mixing length estimate, can be induced by electron scale turbulence.^{53,54} In addition, recent simulations of RF L-mode plasmas at C-Mod have shown that changes in the turbulence and transport due to ETG turbulence must be included with expensive multi-scale simulations (ITG/TEM and ETG together) in order to match the experiment.^{55–57}

In order to investigate the possible role of ETG in the Ohmic L-mode plasmas, linear stability analysis for electron scale turbulence was performed using inputs for the

“ion-heat flux matched” cases in the LOC and SOC discharges. Only electron scale turbulence ($k_y \rho_s = [2.0, 65.0]$ or $k_y \rho_e = [0.0, 1.0]$, where ρ_e is an electron gyroradius, defined as $\rho_e = v_e / \Omega_{ce}$ with $v_e = \sqrt{T_e / m_e}$ and $\Omega_{ce} = eB / m_e c$) was included in these simulations. Ions and electrons are treated as gyrokinetic ions and electrons, and the Debye shielding effect, which can be important for ETG turbulence due to its small spatial scale,^{58,59} is included in the simulation. Boron was used as an impurity with the estimated dilution fraction, and initial value solver was used.

As shown in Fig. 15, the unstable electron modes are found in both discharges. We then varied a/L_{Te} to confirm that these unstable modes are ETG turbulence. It was found that the growth rate of this mode increases with the increase in a/L_{Te} , which is consistent with the characteristics of the ETG turbulence. Although the unstable ETG-like turbulence was found in the linear simulations, the contribution of this unstable mode to electron transport is unknown until multi-scale simulations,^{55,56} which include both ion and electron scale simulations, are performed. This will be future work.

VIII. DISCUSSION AND CONCLUSIONS

In this study, gyrokinetic analysis with the code GYRO was performed to model C-Mod Ohmic L-mode discharges, as part of a study of LOC/SOC transition physics. Detailed comparisons between local, long wavelength electrostatic gyrokinetic simulations and experimental measurements of electron temperature fluctuations have been performed. It was found that GYRO can reproduce Q_i and the synthetic \tilde{T}_e/T_e fluctuation levels within the uncertainty of input parameters, and the \tilde{T}_e/T_e fluctuation spectral shape can also be reproduced within the uncertainty of the measured radial

electric field, E_r . However, Q_e is under-predicted robustly and cannot be recovered by changing the simulation inputs within error bars. Because the long wavelength simulations can match both the ion heat flux (presumably due predominantly to ion-scale turbulence) and the \tilde{T}_e/T_e fluctuation level, which is ion-scale turbulence ($k_y \rho_s < 0.3$), it may be possible to probe the electron heat flux under-prediction and the relevance of ETG turbulence using electron-scale simulations only. However, recent work in C-Mod has shown that multi-scale simulations⁵⁶ are required to accurately model the experiments, since the inclusion of ETG turbulence modifies the interactions between the ITG/TEM scale turbulence and the zonal flows. Both electron-scale and multi-scale simulations will be explored as part of future work.

The non-linear gyrokinetic simulations showed that ion heat transport is enhanced in the SOC discharge compared to the LOC discharge, a trend that was observed in experimental power balance. In contrast, changes in the electron heat transport were small (within error bars). Since it is the increase of ion transport that correlates with the LOC/SOC transition, we note that in the GYRO simulations, we found that the simulated potential and the ion temperature fluctuations also increase in the SOC discharge compared to the LOC discharge. Future work to measure the fluctuations of potential and ion temperature in experiments may shed light on the changes in turbulent ion transport across the LOC/SOC transition.

A primary observation from the experiments is that the electron temperature fluctuation level measured at $r/a \sim 0.85$ is reduced in SOC plasmas compared to LOC plasmas. From the sensitivity analysis, this could be a result of changes in collisionality or changes in turbulence drive (from normalized gradients). While dilution, n_D/n_e , is also higher in the

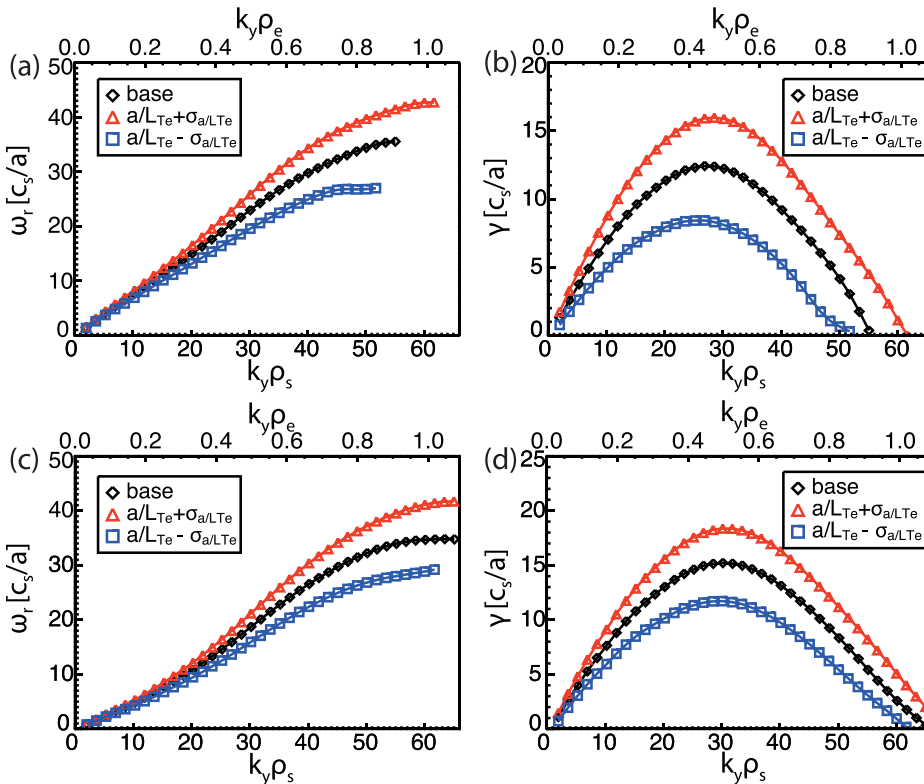


FIG. 15. Linear stability analysis of electron scale turbulence (ETG) for the Q_i matched cases in the LOC/SOC discharges with changes in a/L_{Te} by its uncertainty. (a) Real frequency, ω_r [c_s/a] and growth rate, γ [c_s/a] in the LOC discharge (b) ω_r [c_s/a] and γ [c_s/a] in the SOC discharge.

SOC discharge than in the LOC discharge, we exclude this as the cause for differences in fluctuation levels based on the sensitivity scans. In the scans, an increase of n_D/n_e makes synthetic CECE temperature fluctuation levels higher. So the changes in simulated fluctuations with changes in n_D/n_e are not consistent with the experimental observations that fluctuation levels are reduced. In addition, ν_{ei} is also higher in the SOC discharge compared to the LOC discharge. The increase of ν_{ei} tends to decrease of synthetic CECE temperature fluctuation level, which is consistent with the measurements. Thus, the increase of ν_{ei} can be a reason for the reduction of \tilde{T}_e/T_e fluctuations going from LOC to SOC plasmas. However, it is also possible that slight differences in gradient scale lengths are also a reason for the reduction of \tilde{T}_e/T_e fluctuations. The sensitivity scans show large variations of synthetic CECE \tilde{T}_e/T_e fluctuation level as gradient scale lengths are varied within experimental uncertainties. At this point, the two effects cannot be separated. Thus, while dilution can be ruled out, it remains an open question whether collisionality or one of gradient scale lengths (a/L_T , a/L_{Te} , a/L_n), or a combination of them, is the reason for the reduction of \tilde{T}_e/T_e fluctuations.

The results from this study also addressed the hypothesis that there is a change in the underlying turbulence from dominant trapped electron mode (TEM) to ion temperature gradient (ITG) across the LOC/SOC transition.^{11,12,15} However, we show that there is no evidence of a clear, simple change from TEM to ITG turbulence as density is increased across the LOC/SOC transition based on the results of GYRO simulations, including extensive sensitivity analysis performed on nonlinear simulations. In this study, the simple linear ITG/TEM transition picture is not appropriate for the LOC/SOC transition, since the inner core $r/a = 0.6$ is ITG dominant in both discharges¹³ and the outer core $r/a = 0.85$ is “mixed mode,” with both ITG and TEM unstable. The nonlinear gyrokinetic analysis suggests that the changes in turbulence and heat fluxes across the LOC/SOC transition are due to a variety of factors, but with no change in turbulence propagation or nonlinear mode structure. It is worth noting that there are cases where the LOC/SOC transition is correlated with the changes in dominant turbulence mode from TEM to ITG in gyrokinetic simulations.^{30,50,60} This study also suggests that TEM is relatively more important in the LOC discharge compared to the SOC discharge. However, it is also true that both discharges have “mixed mode” and this study results are not fit into the old hypothesis. We note that there will be no “pure” ITG or TEM turbulence in real experiments and that the non-linear physics is critical to investigate the LOC/SOC transition. Moreover, the new nonlinear GYRO simulations presented here that are constrained to match both the ion heat flux and measured CECE temperature fluctuations strongly suggest that electron scale turbulence (ETG) is important in both the LOC and SOC discharges. Aside from related work at C-Mod¹² and the report of high-k fluctuation measurements from the HT-7 Tokamak,⁶¹ the role of ETG in the LOC/SOC transition has been largely ignored. Overall, these results indicate that the old hypothesis about the LOC/SOC transition should be modified. In these plasmas, there is no evidence of a clear ITG to TEM transition, and there is

evidence suggesting that ETG turbulence plays an important role in Ohmic plasma transport and confinement. In future studies of the LOC/SOC transition and the associated transport changes, the role of ETG should be taken into account.

An interesting additional result from this study is that we found no evidence of the DIII-D-type “Transport Shortfall”³ in Ohmic L-mode plasmas at C-Mod. The “Shortfall” is when both ion and electron heat fluxes, and fluctuation levels, are under-predicted by the simulations. In our plasmas, the ion heat flux and electron temperature fluctuation levels are matched, and only the electron heat flux is under-predicted. Past work at C-Mod showed that RF heated L-mode plasmas did not exhibit the transport shortfall.²² The absence of a “Shortfall” in C-Mod Ohmic L-mode plasmas as reported here is further evidence that the “Shortfall” observed at DIII-D is (1) not universal across tokamaks and (2) is not due to issues with GYRO at least within the parameter regime studied in this paper, i.e., in the C-Mod Ohmic discharges with low rotation compared to other machines. Instead, it appears to be specific to low-power NBI heated L-mode discharges at DIII-D and is an area of active research within the transport community.

ACKNOWLEDGMENTS

The authors would like to thank J. E. Rice, M. L. Reinke, and C. Gao for HIREX analysis, J. Walk and J. W. Hughes for Thomson Scattering analysis, A. E. Hubbard for GPC analysis, and S. Wolfe for EFIT analysis. Experimental work was supported by the U.S. Department of Energy Grant Nos. DE-SC0006419 and DE-FC02-99ER54512. Special thanks to J. Wright and T. Baker for maintaining the LOKI computer cluster used for linear GYRO simulations. The nonlinear GYRO simulations were carried out at the National Energy Research Scientific Computing Center, supported by the Office of Science of the U.S. Department of Energy under Contract No. DE-AC02-05CH11231.

¹G. R. Tynan, A. Fujisawa, and G. McKee, *Plasma Phys. Controlled Fusion* **51**, 113001 (2009).

²A. E. White, L. Schmitz, W. A. Peebles, T. A. Carter, T. L. Rhodes, E. J. Doyle, P. A. Gourdain, J. C. Hillesheim, G. Wang, C. Holland *et al.*, *Rev. Sci. Instrum.* **79**, 103505 (2008).

³C. Holland, A. E. White, G. R. McKee, M. W. Shafer, J. Candy, R. E. Waltz, L. Schmitz, and G. R. Tynan, *Phys. Plasmas* **16**, 052301 (2009).

⁴A. Casati, T. Gerbaud, P. Hennequin, C. Bourdelle, J. Candy, F. Clairet, X. Garbet, V. Grandgirard, Ö. Gürçan, S. Heuraux *et al.*, *Phys. Rev. Lett.* **102**, 165005 (2009).

⁵A. E. White, W. A. Peebles, T. L. Rhodes, C. H. Holland, G. Wang, L. Schmitz, T. A. Carter, J. C. Hillesheim, E. J. Doyle, L. Zeng, G. R. McKee, G. M. Staebler, R. E. Waltz, J. C. DeBoo, C. C. Petty, and K. H. Burrell, *Phys. Plasmas* **17**, 056103 (2010).

⁶T. L. Rhodes, C. Holland, S. P. Smith, A. E. White, K. H. Burrell, J. Candy, J. C. DeBoo, E. J. Doyle, J. C. Hillesheim, J. E. Kinsey *et al.*, *Nucl. Fusion* **51**, 063022 (2011).

⁷T. Görler, A. E. White, D. Told, F. Jenko, C. Holland, and T. L. Rhodes, *Phys. Plasmas* **21**, 122307 (2014).

⁸A. R. Field, D. Dunai, Y. C. Ghim, P. Hill, B. McMillan, C. M. Roach, S. Saarelma, A. A. Schekochihin, S. Zoletnik, and MAST Team, *Plasma Phys. Controlled Fusion* **56**, 025012 (2014).

⁹L. Lin, M. Porkolab, E. M. Edmund, M. Greenwald, N. Tsujii, J. Candy, R. E. Waltz, and D. R. Mikkelsen, *Plasma Phys. Controlled Fusion* **51**, 065006 (2009).

- ¹⁰P. Ennever, M. Porkolab, J. Candy, G. Staebler, M. L. Reinke, J. E. Rice, J. C. Rost, D. Ernst, C. Fiore, J. Hughes, J. Terry, and Alcator C-Mod Team, *Phys. Plasmas* **22**, 072507 (2015).
- ¹¹J. E. Rice, C. Gao, M. L. Reinke, P. H. Diamond, N. T. Howard, H. J. Sun, I. Cziegler, A. E. Hubbard, Y. A. Podpaly, W. L. Rowan, J. L. Terry, M. A. Chilenski, L. Delgado-Aparicio, P. C. Ennever, D. Ernst, M. J. Greenwald, J. W. Hughes, Y. Ma, E. S. Marmor, M. Porkolab, A. E. White, and S. M. Wolfe, *Nucl. Fusion* **53**, 033004 (2013).
- ¹²C. Gao, J. E. Rice, H. J. Sun, M. L. Reinke, N. T. Howard, D. Mikkelsen, A. E. Hubbard, M. A. Chilenski, J. Walk, J. W. Hughes *et al.*, *Nucl. Fusion* **54**, 083025 (2014).
- ¹³C. Sung, A. E. White, N. T. Howard, C. Y. Oi, J. E. Rice, C. Gao, P. Ennever, M. Porkolab, F. Parra, D. Mikkelsen *et al.*, *Nucl. Fusion* **53**, 083010 (2013).
- ¹⁴R. M. McDermott, C. Angioni, G. D. Conway, R. Dux, E. Fable, R. Fischer, T. Pütterich, F. Ryter, and ASDEX Upgrade Team, *Nucl. Fusion* **54**, 043009 (2014).
- ¹⁵J. E. Rice, B. P. Duval, M. L. Reinke, Y. A. Podpaly, A. Bortolon, R. M. Churchill, I. Cziegler, P. H. Diamond, A. Dominguez, P. C. Ennever, C. L. Fiore, R. S. Granetz, M. J. Greenwald, A. E. Hubbard, J. W. Hughes, J. H. Irby, Y. Ma, E. S. Marmor, R. M. McDermott, M. Porkolab, N. Tsujii, and S. M. Wolfe, *Nucl. Fusion* **51**, 083005 (2011).
- ¹⁶J. Bernardo, C. Fenzi, C. Bourdelle, Y. Camenen, H. Arnichand, J. P. S. Bizarro, S. Cortes, X. Garbet, Z. O. Guimarães-Filho, T. Aniel *et al.*, *Plasma Phys. Controlled Fusion* **57**, 035002 (2015).
- ¹⁷C. Angioni, R. M. McDermott, F. J. Casson, E. Fable, A. Bottino, R. Dux, R. Fischer, Y. Podoba, T. Pütterich, F. Ryter *et al.*, *Phys. Rev. Lett.* **107**, 215003 (2011).
- ¹⁸J. Candy and R. E. Waltz, *J. Comput. Phys.* **186**, 545 (2003).
- ¹⁹See <http://w3.pppl.gov/transp/> for “Transp homepage,” 2014.
- ²⁰C. Sung, A. E. White, J. H. Irby, R. Leccacorvi, R. Vieira, C. Y. Oi, W. A. Peebles, and X. Nguyen, *Rev. Sci. Instrum.* **83**, 10E311 (2012).
- ²¹N. T. Howard, A. E. White, and C. Sung, *Rev. Sci. Instrum.* **85**, 11D811 (2014).
- ²²N. T. Howard, A. E. White, M. Greenwald, M. L. Reinke, J. Walk, C. Holland, J. Candy, and T. Görler, *Phys. Plasmas* **20**, 032510 (2013).
- ²³D. Told, F. Jenko, T. Görler, F. J. Casson, E. Fable, and ASDEX Upgrade Team, *Phys. Plasmas* **20**, 122312 (2013).
- ²⁴G. Cima, R. V. Bravenec, A. J. Wootton, T. D. Rempel, R. F. Gandy, and C. Watts, *Phys. Plasmas* **2**, 720 (1995).
- ²⁵L. Porte, S. Coda, T. P. Goodman, A. Pochelon, V. S. Udintsev, and V. Vuille, in *EPJ Web of Conferences* (EDP Sciences, 2012), Vol. 32, p. 03007.
- ²⁶C. Sung, “Experimental study of turbulent heat transport in Alcator C-Mod,” Ph.D. thesis, MIT, 2015.
- ²⁷J. M. Schachter, “Local transport analysis for the alcator C-Mod tokamak,” Ph.D. thesis, MIT, 1997.
- ²⁸L. L. Lao, H. S. John, R. D. Stambaugh, A. G. Kellman, and W. Pfeiffer, *Nucl. Fusion* **25**, 1611 (1985).
- ²⁹F. Wagner and U. Stroth, *Plasma Phys. Controlled Fusion* **35**, 1321 (1993).
- ³⁰C. L. Rettig, T. L. Rhodes, J. N. Leboeuf, W. A. Peebles, E. J. Doyle, G. M. Staebler, K. H. Burrell, and R. A. Moyer, *Phys. Plasmas* **8**, 2232 (2001).
- ³¹J. E. Rice, M. J. Greenwald, Y. A. Podpaly, M. L. Reinke, P. H. Diamond, J. W. Hughes, N. T. Howard, Y. Ma, I. Cziegler, B. P. Duval, P. C. Ennever, D. Ernst, C. L. Fiore, C. Gao, J. H. Irby, E. S. Marmor, M. Porkolab, N. Tsujii, and S. M. Wolfe, *Phys. Plasmas* **19**, 056106 (2012).
- ³²F. Romanelli and S. Briguglio, *Phys. Fluids B* **2**, 754 (1990).
- ³³J. W. Connor and H. R. Wilson, *Plasma Phys. Controlled Fusion* **36**, 719 (1994).
- ³⁴S. Migliuolo, *Nucl. Fusion* **33**, 3 (1993).
- ³⁵G. R. McKee, M. Murakami, J. A. Boedo, N. H. Brooks, K. H. Burrell, D. R. Ernst, R. J. Fonck, G. L. Jackson, M. Jakubowski, R. J. L. Haye *et al.*, *Phys. Plasmas* **7**, 1870 (2000).
- ³⁶B. Esposito, M. Marinucci, G. Bracco, C. Castaldo, V. Cocilovo, E. Giovannozzi, M. Leigh, G. Monari, S. Nowak, C. Sozzi, O. Tudisco, R. Cesario, D. Frigione, G. Gormezano, G. Granucci, L. Panaccione, V. Pericoli-Ridolfini, L. Pieroni, and FTU and ECRH Teams, *Plasma Phys. Controlled Fusion* **46**, 1793 (2004).
- ³⁷X. Garbet, J. Payan, C. Laviron, P. Devynck, S. K. Saha, H. Capes, X. P. Chen, J. P. Coulon, C. Gil, G. R. Harris, T. Hutter, and A. L. Pecquet, *Nucl. Fusion* **32**, 2147 (1992).
- ³⁸R. L. Miller, M. S. Chu, J. M. Greene, Y. R. Lin-Liu, and R. E. Waltz, *Phys. Plasmas* **5**, 973 (1998).
- ³⁹N. T. Howard, M. Greenwald, D. R. Mikkelsen, M. L. Reinke, A. E. White, D. Ernst, Y. Podpaly, and J. Candy, *Nucl. Fusion* **52**, 063002 (2012).
- ⁴⁰R. V. Bravenec and W. M. Nevins, *Rev. Sci. Instrum.* **77**, 015101 (2006).
- ⁴¹M. Porkolab, J. Dorris, P. Ennever, C. Fiore, M. Greenwald, A. Hubbard, Y. Ma, E. Marmor, Y. Podpaly, M. L. Reinke *et al.*, *Plasma Phys. Controlled Fusion* **54**, 124029 (2012).
- ⁴²R. M. McDermott, B. Lipschultz, J. W. Hughes, P. J. Catto, A. E. Hubbard, I. H. Hutchinson, R. S. Granetz, M. Greenwald, B. LaBombard, K. Marr *et al.*, *Phys. Plasmas* **16**, 056103 (2009).
- ⁴³W. A. Houlberg, K. C. Shaing, S. P. Hirshman, and M. C. Zarnstorff, *Phys. Plasmas* **4**, 3230 (1997).
- ⁴⁴W. M. Solomon, K. H. Burrell, R. Andre, L. R. Baylor, R. Budny, P. Gohil, R. J. Groebner, C. T. Holcomb, W. A. Houlberg, and M. R. Wade, *Phys. Plasmas* **13**, 056116 (2006).
- ⁴⁵C. Chrystal, K. H. Burrell, B. A. Grierson, R. J. Groebner, and D. H. Kaplan, *Rev. Sci. Instrum.* **83**, 10D501 (2012).
- ⁴⁶B. A. Grierson, K. H. Burrell, W. W. Heidbrink, M. J. Lanctot, N. A. Pablant, and W. M. Solomon, *Phys. Plasmas* **19**, 056107 (2012).
- ⁴⁷C. Theiler, R. M. Churchill, B. Lipschultz, M. Landreman, D. R. Ernst, J. W. Hughes, P. J. Catto, F. I. Parra, I. H. Hutchinson, M. L. Reinke *et al.*, *Nucl. Fusion* **54**, 083017 (2014).
- ⁴⁸R. M. Churchill, C. Theiler, B. Lipschultz, I. H. Hutchinson, M. L. Reinke, D. Whyte, J. W. Hughes, P. Catto, M. Landreman, D. Ernst *et al.*, *Phys. Plasmas* **22**, 056104 (2015).
- ⁴⁹D. Ernst *et al.*, in 25th IAEA Conference on Fusion Energy (IAEA, 2014).
- ⁵⁰H. Arnichand, R. Sabot, S. Hacquin, A. Krämer-Flecken, X. Garbet, J. Citrin, C. Bourdelle, G. Hornung, J. Bernardo, C. Bottereau *et al.*, *Nucl. Fusion* **54**, 123017 (2014).
- ⁵¹J. M. Candy, *Bull. Am. Phys. Soc.* **60** (2015), available at <http://meetings.aps.org/link/BAPS.2015.DPP.GI2.1>.
- ⁵²See <https://fusion.gat.com/theory/gyrousermanual> for “GYRO web page,” 2013.
- ⁵³F. Jenko, W. Dorland, M. Kotschenreuther, and B. N. Rogers, *Phys. Plasmas* **7**, 1904 (2000).
- ⁵⁴W. Dorland, F. Jenko, M. Kotschenreuther, and B. N. Rogers, *Phys. Rev. Lett.* **85**, 5579 (2000).
- ⁵⁵N. T. Howard, C. Holland, A. E. White, M. Greenwald, and J. Candy, *Phys. Plasmas* **21**, 112510 (2014).
- ⁵⁶N. T. Howard, C. Holland, A. E. White, M. Greenwald, and J. Candy, *Plasma Phys. Controlled Fusion* **57**, 065009 (2015).
- ⁵⁷N. T. Howard, C. Holland, A. E. White, M. Greenwald, and J. Candy, *Nucl. Fusion* **56**, 014004 (2015).
- ⁵⁸F. Jenko, W. Dorland, and G. W. Hammett, *Phys. Plasmas* **8**, 4096 (2001).
- ⁵⁹Y. Idomura, M. Wakatani, and S. Tokuda, *Phys. Plasmas* **7**, 2456 (2000).
- ⁶⁰H. Arnichand, J. Citrin, S. Hacquin, R. Sabot, A. Krämer-Flecken, X. Garbet, C. Bourdelle, C. Bottereau, F. Claret, J. C. Giacalone *et al.*, *Plasma Phys. Controlled Fusion* **58**, 014037 (2016).
- ⁶¹T. Zhang, X. Gao, Y. Li, and J. Zhao, *Phys. Lett. A* **372**, 4705 (2008).
- ⁶²E. S. Marmor *et al.*, *Nucl. Fusion* **49**, 104014 (2009).